Synthesis, Structure, and Magnetic and Mössbauer Properties of Mononuclear and Asymmetric, Oxo-Bridged Trinuclear Iron(III) Complexes of a New Polyimidazole Ligand

Sergiu M. Gorun,[1a] Georgia C. Papaefthymiou,[1b] Richard B. Frankel,[1b] and Stephen J. Lippard*[1a]

Contribution from the Department of Chemistry and the Francis Bitter National Magnet Laboratory, Massachusetts Institute of Technology, Cambridge, Massachusetts 02139.
Received August 8, 1986

Abstract: The synthesis of 1,1,2-tris(*N*-methylimidazol-2-yl)-1-hydroxyethane (TIEOH) is described. Reaction of TIEOH with $Fe(ClO_4)_3 \cdot 10H_2O$ yields, upon workup and crystallization, the high-spin, pseudooctahedral iron(III) monomer $[Fe(TIEO)(HTIEO)](ClO_4)_2$, in which two imidazole ring nitrogen atoms and an alkoxide oxygen atom of both $TIEO^-$ and HTIEO ligands are coordinated to the metal. The dangling imidazole of the HTIEO ligand is protonated, as revealed in an X-ray crystal structure determination. Two procedures are described for preparing the novel trinuclear complex $[Fe_3O(TIEO)_2(O_2CPh)_2Cl_3] \cdot 2C_6H_6$. This trinuclear complex slowly decomposes in solution to form $[Fe(BIK)_3]^{2+}$, where BIK is bis(*N*-methylimidazol-2-yl) ketone. An X-ray crystallographic study of the trinuclear complex revealed an isosceles triangle of iron atoms with a triply bridging oxo atom nearly in the plane of the triangle. The structure of the $\{Fe_3O\}^{7+}$ core consists of two short Fe-O bonds [Fe1-O3, 1.862 (7) Å; Fe2-O3, 1.867 (7) Å; Fe1-O3-Fe2, 159.1 (3)°] and one long one [Fe3-O3, 2.067 (6) Å; Fe1-O3-Fe3, 100.3 (3)°; Fe2-O3-Fe3, 100.5 (3)°]. The coordination spheres of the equivalent iron atoms, Fe1 and Fe2, are each composed of two imidazole nitrogen atoms, the bridging oxo atom, a bridging alkoxide oxygen atom of the $TIEO^-$ ligand, an oxygen atom of a bridging benzoate ligand, and a terminal chloride ion. The two benzoate, two alkoxide, and μ-oxo groups bridge to Fe3, which has a terminal chloride ligand to complete its coordination sphere. Two *N*-methylimidazole groups, one from each ligand, are not coordinated. From magnetization studies the ground state of $[Fe_3O(TIEO)_2(O_2CPh)_2Cl_3]$ is found to be $S_T = {}^5/_2$, in contrast to the classical basic iron(III) carboxylates, which contain symmetrically bridged $\{Fe_3O\}^{7+}$ cores having $S_T = {}^1/_2$. Variable-temperature magnetic susceptibility measurements were fit to a theoretical expresssion derived from a spin Hamiltonian taking into account two different exchange pathways along inequivalent sides of the isosceles triangle. The analysis yielded $J_{12} = -55$ (1) cm^{-1} and $J_{13} = J_{23} = -8.0$ (4) cm^{-1}, with the large antiferromagnetic coupling interaction occurring between iron centers linked by the shortest μ-oxo bridge bonds. Mössbauer isomer shift and quadrupole splitting parameters at 4.2 K are δ 0.48 and 0.52 mm/s and $\Delta E_Q = 1.16$ and 0.74 mm/s for Fe1 (= Fe2) and Fe3, respectively. In external magnetic fields at 4.2 K there are two magnetic subsites with $H_{hf}(1) = H_{hf}(2) = 0$ and $H_{hf}(3) = -540$ kOe, corresponding to Fe1 and Fe2 with local spin $\langle S_z \rangle = 0$ and Fe3 with local spin $\langle S_z \rangle = {}^5/_2$. This result confirms the $|S_T = {}^5/_2, S_p = 0\rangle$ ground state of the cluster. Electronic, vibrational, and NMR spectra are also briefly reported. These results are compared and contrasted with structural, magnetic, and spectroscopic data for (μ-oxo)diiron(III), (μ-hydroxy)diiron(III), and symmetric (μ_3-oxo)triiron(III) cores which, unlike the present asymmetric (μ_3-oxo)triiron(III) core, are ubiquitous in mineralogy and biology.

Oxo-bridged polyiron centers are widespread in the mineralogical and biological worlds. Discrete binuclear centers occur in the oxygen transport proteins hemerythrin (Hr), found in marine invertebrates,[2] in ribonucleotide reductase (RR),[3] and in purple acid phosphatases.[4] Polynuclear iron centers, found in the iron storage proteins ferritin (Ft) and hemosiderin,[5] are also involved in the formation of magnetic crystals in magnetotactic organisms[6] and chitons.[7] As discrete units, oxo-bridged trinuclear iron centers are thus far unknown in biology but are likely intermediates in the formation of larger polynuclear iron aggregates. The $\{Fe_3O\}^{7+}$ unit has been proposed as the smallest building block of the ferritin core.[8]

Inorganic chemists have been interested in oxo-bridged trinuclear iron centers for over a century,[9] especially the symmetric (μ_3-oxo)triiron(III) core shown below, where L is H_2O or pyridine and R is an alkyl or aryl group, that occurs in the "basic iron

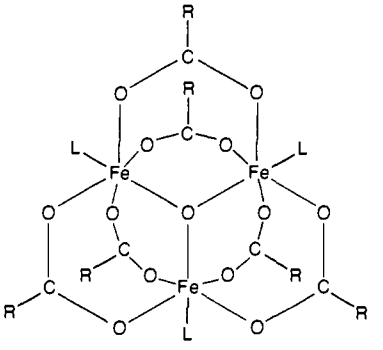

acetates".[8,10] Several mixed-valence,[11] heterometallic,[12] and

(1) (a) Department of Chemistry. (b) Francis Bitter National Magnet Laboratory.

(2) (a) Klotz, I. M.; Kurtz, D. M., Jr. *Acc. Chem. Res.* **1984**, *17*, 16-22. (b) Hendrickson, W. A. in *Invertebrate Oxygen-Binding Proteins: Structure, Active Site and Function*; Lamy, J., Lamy, J., Eds.; Marcel-Dekker: New York, 1981; pp 503-515. (c) Stenkamp, R. E.; Sieker, L. C.; Jensen, L. H. *J. Am. Chem. Soc.* **1984**, *106*, 618-622.

(3) (a) Reichard, P.; Ehrenberg, A. *Science (Washington, D.C.)* **1983**, *221*, 514-519. (b) Sjöberg, B.-M.; Gräslund, A. *Adv. Inorg. Biochem.* **1983**, *5*, 87-110.

(4) (a) Davis, J. C.; Averill, B. A. *Proc. Natl. Acad. Sci. U.S.A.* **1982**, *79*, 4623-4627. (b) Sinn, E.; O'Connor, C. J.; de Jersey, J.; Zerner, B. *Inorg. Chim. Acta* **1983**, *78*, L13-L15. (c) Antanaitis, B. C.; Aisen, P.; Lilienthal, H. R. *J. Biol. Chem.* **1983**, *258*, 3166-3172.

(5) (a) Theil, E. C. *Adv. Inorg. Biochem.* **1983**, *5*, 1-38. (b) Ford, G. C.; Harrison, P. M.; Rice, D. W.; Smith, J. M. A.; Treffry, A.; White, J. L.; Yariv, J. *Phil. Trans. R. Soc. London, Ser. B* **1984**, *304*, 551-565. (c) Aisen, P.; Listowsky, I. *Annu. Rev. Biochem.* **1980**, *49*, 357-393.

(6) Frankel, R. B.; Blakemore, R. P.; Wolfe, R. S. *Science (Washington, D.C.)* **1979**, *203*, 1355-1357.

(7) Lowenstam, H. A. *Science (Washington, D.C.)* **1981**, *211*, 1126-1130.

(8) (a) Holt, M. E.; Holt, S. L.; Tucker, W. F.; Asplund, R. D.; Watson, K. J. *J. Am. Chem. Soc.* **1974**, *96*, 2621-2623. (b) Heald, S. M.; Stearn, E. A.; Bunker, B.; Holt, E. M.; Holt, S. L. *J. Am. Chem. Soc.* 1979, *101*, 67-73.

(9) (a) Weinland, R. F.; Hohn, A. *Z. Anorg. Chem.* **1926**, *152*, 1-15. (b) Welo, L. A. *Philos. Mag. S7* **1928**, *6*, 481-509. (c) Scheurer-Kestner, M. *Ann. Chim. Phys.* **1861**, *Ser. 3*, *63*, 422-447.

(10) (a) Holt, E. M.; Holt, S. L.; Alcock, N. W. *Cryst. Struct. Commun.* **1982**, *11*, 505-508. (b) Dziobkowski, C. T.; Wrobleski, J. T.; Brown, D. B. *Inorg. Chem.* **1981**, *20*, 671-678. (c) Catterick, J.; Thornton, P. *Adv. Inorg. Chem. Radiochem.* **1977**, *20*, 291-362. (d) Cotton, F. A.; Wilkinson, G. *Advanced Inorganic Chemistry*; Wiley: New York, 1980; pp 154-155.

(11) (a) Sorai, M.; Kaji, K.; Hendrickson, D. N.; Oh, S. M. *J. Am. Chem. Soc.* **1986**, *108*, 702-708. (b) Oh, S. M.; Hendrickson, D. M.; Hassett, K. L.; Davis, R. E. *J. Am. Chem. Soc.* **1985**, *107*, 8009-8018. (c) Cannon, R. D.; Montri, L.; Brown, D. B.; Marshall, K. M.; Elliott, C. M. *J. Am. Chem. Soc.* **1984**, *106*, 2591-2594. (d) Turtê, K. I.; Bobkova, S. A. Stukan, R. A.; Dorogan, A. V.; Veksel'man, M. E. *Koord. Khim.* **1982**, *8*, 794-800.

0002-7863/87/1509-4244$01.50/0

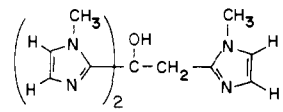

TIEOH

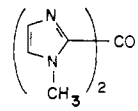

BIK

Figure 1. Structures of two polyimidazole ligands used in this study and their abbreviations.

sulfate-bridged[13] analogues have also been studied.

The discovery of an unusual asymmetric (μ_3-oxo)triiron(III) core in our laboratory[14] occurred during attempts to extend previous work on the hemerythrin model compound $[Fe_2O(O_2CCH_3)_2(HBpz_3)_2]$[15] and its derivatives,[16] where $HBpz_3^-$ = hydrotris(1-pyrazolyl)borate. Specifically, we wanted to replace polypyrazole with biologically more relevant polyimidazole ligands and to build functional models for the binuclear centers in Hr and RR. The synthesis of higher nuclearity polyiron complexes was an additional objective. Since the coordination chemistry of iron with polyimidazole ligands was unknown prior to our studies, several mononuclear complexes were also synthesized and characterized.[17]

In the present report we describe the synthesis of a new polyimidazole ligand TIEOH, 1,1,2-tris(1-methylimidazol-2-yl)ethanol (Figure 1), and the preparation and properties of the mononuclear complex $[Fe(TIEO)(TIEOH)](ClO_4)_2$. The primary focus, however, is on the compound $[Fe_3O(TIEO)_2(O_2CPh)_2Cl_3]\cdot 2C_6H_6$, a trinuclear iron oxo cluster containing an asymmetric $\{Fe_3O\}^{7+}$ core having unique magnetic and Mössbauer properties that reflect its unusual molecular structure.

Experimental Section

Materials and Methods. Preparation of Compounds. Solvents and reagents were obtained from commercial sources and used without purification unless otherwise noted. Tetrahydrofuran (THF) was dried by distillation from potassium/benzophenone. Acetonitrile and benzene were dried by distilling them from calcium hydride. Anhydrous ether was stirred over Na for 10 min prior to use. *N*-Methylimidazole was of reported 99% purity. 1,2-Dimethylimidazole was recrystallized from benzene. Triethylamine was distilled from phenyl isocyanate and stored over KOH. $(Et_4N)_2[Fe_2OCl_6]$ was prepared by a literature procedure.[18] $(Et_4N)[FeCl_4]$ was prepared from $FeCl_3\cdot 6H_2O$ and Et_4NCl by a method similar to that employed for its Fe(II) analogue.[19] Elemental analyses were performed by Atlantic Microlabs, Inc., Atlanta, GA.

Bis(*N*-methylimidazol-2-yl) Ketone (BIK), 1. A 1-L, three-necked, flame-dried round-bottomed flask was charged under N_2 with 360 mL of anhydrous ether and 12.5 mL (0.157 mol) of *N*-methylimidazole and then cooled to −78 °C in a dry ice–acetone bath. A 2.5 M solution of *n*-butyllithium in hexanes (60.0 mL, 0.15 mol) was added via syringe, and the mixture was stirred for 2 h at −65 °C. Stirring was continued for 0.5 h at −40 °C, after which the mixture was cooled to −78 °C and added by cannula to a precooled solution of 6.06 mL (0.05 mol) of diethyl carbonate in 50 mL of THF over a period of 1 h. The mixture was allowed to warm to −45 °C in 1.5 h, excess solid CO_2 was added, and the reaction was allowed to reach room temperature overnight. The solvents were removed in vacuo, the residue was dissolved in 600 mL of brine, and the solution was extracted with methylene chloride. The organic layer was dried over Na_2SO_4; the solvents were removed, and the remaining solid was washed twice with 1 mL of cold acetone in order to remove unreacted imidazole. Recrystallization from boiling acetone gave, after drying, 7.24 g (76%) of **1** as a white powder. Its spectroscopic properties agreed with literature data.[20] Mass spectrum (FAB): *m/e* 191.09 (MH^+). Anal. Calcd for $C_9H_{10}N_4O$: C, 56.83; H, 5.30; N, 29.46. Found: C, 56.88; H, 5.31; N, 29.28.

1,1,2-Tris(*N*-methylimidazol-2-yl)-1-hydroxyethane (TIEOH), 2. A flame-dried, 1-L, 3-necked round-bottomed flask was charged with 2.44 g (25.4 mmol) of 1,2-dimethylimidazole and 175 mL of THF, and the solution was cooled to −78 °C. A 2.5 M solution of *n*-butyllithium in hexanes (9.8 mL, 24.5 mmol) was added via syringe, and the mixture was allowed to warm to −40 °C in 1.5 h. The flask was cooled to −78 °C, and a solution of 3.87 g (20.3 mmol) of BIK (**1**) in 600 mL of THF was added via cannula over a period of 3 h. The temperature should not exceed −70 °C during this transfer. The reaction mixture was allowed to warm to room temperature overnight and stirred an additional 36 h. H_2O (50 mL) was added afterward, and the stirring was continued for 10 min, followed by removal of the solvents in vacuo, addition of brine, extraction with CH_2Cl_2, drying of the organic phase over K_2CO_3, and rotoevaporation of the solvent. The yellowish solid left was triturated with ether, filtered, and recrystallized from benzene to give 2.53 g (43% yield) of **2** as a white crystalline material: mass spectrum (EI, 70 eV), *m/e* 286 (M^+), (FAB) 287 (MH^+); mp (uncorrected) 189 °C; IR (KBr, cm^{-1}) 3200–3400 (br), 3080 (m), 1470 (s), 1390 (m), 1280 (s), 1240 (s), 1200, 1145 (s), 1090 (m), 1080 (m) 1005, 935, 920, 780 (m), 755 (s), 730 (m), 680, 660, 600, 570, 540, 500. ^1H NMR (270 MHz, $CDCl_3$): δ 6.84–6.85 (CH, 2 H), 6.75–6.76 (CH, OH, 4 H), 6.73 (CH, 1 H), 3.77 (CH_2, 2 H), 3.60 (CH_3 3 H), 3.53 (CH_3, 6 H). Anal. Calcd for $C_{14}H_{18}N_6O$: C, 58.73; H, 6.34; N, 29.35. Found: C, 58.23; H, 6.38; N, 28.94.

(1,1,2-Tris(*N*-methylimidazol-2-yl)ethane 1-oxide-*N*,*N*,*O*)(1,2-bis(*N*-methylimidazol-2-yl)-1-(*N*-methyl-*N*′-protioimidazol-2-yl)ethane 1-oxide-*N*,*N*,*O*)iron(III) Perchlorate, [Fe(TIEO)(HTIEO)](ClO$_4$)$_2$, 3. To a solution of 0.0467 g (0.087 mmol) of $Fe(ClO_4)_3\cdot 10H_2O$ in 0.5 mL of H_2O was added 0.0505 g (0.176 mmol) of solid TIEOH (**2**) while stirring rapidly. The solution turned orange and a bright-yellow solid precipitated. After an additional 10 min of stirring, the precipitate was filtered. The pH of the filtrate was 1.5. The precipitate was dried under vacuum over P_4O_{10} overnight to give 0.061 g (91%) of **3** as a yellow powder. Crystallization by slow evaporation from aqueous $HClO_4$ at pH 1 gave crystals of $3\cdot 4H_2O$, which was fully characterized by X-ray diffraction (vide infra). IR (KBr, cm^{-1}): 3420 (br, s), 3230, 3160, 2920, 1490 (m), 1285 (m), 1100 (vs), 1020 (m), 995 (m), 960 (m) 915, 890, 770, 750 (m), 690 (m), 670, 625 (m), 570 (m), 520, 420, 400. Solid-state effective magnetic moment of desolvated **3** at 296 K: 6.0 μ_B. UV–vis (MeCN): 343, 476 (sh) nm.

(μ_3-Oxo)bis(μ-benzoato)bis(μ-(1,1,2-tris(*N*-methylimidazol-2-yl)-ethane 1-oxide-*N*,*N*,*O*))trichlorotriiron(III) Dibenzene, [Fe$_3$O(TIEO)$_2$-(O$_2$CPh)$_2$Cl$_3$]·2C$_6$H$_6$, 4·2C$_6$H$_6$. Method A. A 0.207-g (0.344-mmol) portion of $(Et_4N)_2[Fe_2OCl_6]$ was dissolved in 3.3 mL of MeCN, and 0.100 g (0.694 mmol) of anhydrous sodium benzoate was added with vigorous stirring. After 2.5 h a slurry of 0.197 g (0.688 mmol) of TIEOH (**2**) in 5.2 mL of CH_2Cl_2 was added dropwise and the mixture was stirred for an additional 2 h. After a white precipitate was removed by filtration, CH_2Cl_2 and benzene were added and removed in vacuo twice. A portion of the brown solid that resulted was dissolved in dry MeCN, yielding a solution in which the iron concentration was 30 mM. Dry benzene was layered on top and allowed to diffuse into the solution. The volume ratio of MeCN to benzene was 3:20. X-ray quality crystals were harvested after 3 weeks.

Method B. To a rapidly stirred solution containing 0.202 g (0.336 mmol) of $(Et_4N)_2[Fe_2OCl_6]$ in 10 mL of MeCN were added 0.110 g (0.335 mmol) of $(Et_4N)[FeCl_4]$ and, after 5 min, 0.097 g (0.673 mmol) of anhydrous $Na(O_2CPh)$ were added to form a brown suspension. After 1 h a solution containing 0.195 g (0.681 mmol) of TIEOH and 0.20 mL (1.4 mmol) of Et_3N dissolved in 15 mL of MeCN was added dropwise over a 5-min period to the brown suspension. The color turned deep red-brown. After 30 min of stirring a white solid was filtered off and the solvent was removed in vacuo. Several successive additions and removals of MeCN allowed the separation of more white solid. Liquid–liquid diffusion of benzene into an acetonitrile solution of crude **4** following the procedure employed in method A gave $4\cdot 2C_6H_6$ in 63% yield. IR (KBr, cm^{-1}): 3122, 2923, 2875, 1598 (m), 1542 (s), 1493 (m), 1400 (vs), 1284 (m), 1160 (m), 1088 (s), 1022 (m), 986, 956, 915, 894, 725 (m), 687, 674, 536, 471 (m), 400. UV–vis ($4\cdot 2C_6H_6$ in MeCN): 272 (sh), 281

(12) For leading references see: Straughan, B. P.; Lam, O. M. *Inorg. Chim. Acta* **1985**, *98*, 7–10.
(13) Thich, J. A.; Toby, B. H.; Powers, D. A.; Potenza, J. A.; Schugar, H. J. *Inorg. Chem.* **1981**, *20*, 3314–3317 and references cited therein.
(14) Gorun, S. M.; Lippard, S. J. *J. Am. Chem. Soc.* **1985**, *107*, 4568–4570.
(15) Armstrong, W. H.; Spool, A.; Papaefthymiou, G. C.; Frankel, R. B.; Lippard, S. J. *J. Am. Chem. Soc.* **1984**, *106*, 3653–3667.
(16) (a) Armstrong, W. H.; Lippard, S. J. *J. Am. Chem. Soc.* **1984**, *106*, 4632–4633. (b) Armstrong, W. H.; Lippard, S. J. *J. Am. Chem. Soc.* **1985**, *107*, 3730–3731.
(17) (a) Gorun, S. M. Ph.D. Thesis, Massuchesetts Institute of Technology, Cambridge, MA, 1986. (b) Gorun, S. M.; Lippard, S. J., to be submitted for publication.
(18) Armstrong, W. H.; Lippard, S. J. *Inorg. Chem.* **1985**, *24*, 981–982.
(19) Gill, N. S.; Taylor, F. B. *Inorg. Synth.* **1967**, *9*, 136–142.
(20) Regel, E.; Buchel, K.-H. *Liebigs Ann. Chem.* **1977**, 145–148.

Table I. Experimental Details of the X-ray Crystallographic Studies of $[Fe(TIEO)(HTIEO)](ClO_4)_2 \cdot 4H_2O$ ($3 \cdot 4H_2O$) and $[Fe_3O(TIEO)_2(O_2CPh)_2Cl_3] \cdot 2C_6H_6$ ($4 \cdot 2C_6H_6$)

(A) Crystal Parameters[a]

	3	4		3	4
a, Å	10.514 (2)	14.080 (1)	space group	$P\bar{1}$	$P\bar{1}$
b, Å	14.170 (2)	15.879 (2)	Z	2	2
c, Å	14.374 (2)	14.043 (2)	ρ_{calcd}, g cm^{-3}	1.535	1.470
α, deg	99.24 (1)	92.50 (1)	ρ_{obsd},[b] g cm^{-3}	1.51 (1)	1.46 (1)
β, deg	97.85 (1)	100.296 (8)	mol wt	898.5	1259.0
γ, deg	109.96 (1)	67.095 (7)			
vol, Å^3	1944.0 (6)	2844.4 (8)			

(B) Measurement and Treatment of Intensity Data

Instrument: Enraf-Nonius CAD-4F κ-Geometry Diffractometer
Radiation: Mo Kα (λ_α = 0.71073 Å, Graphite Monochromatized)

	3	4
no. of reflctns collected	8079 ($3° \le 2\theta \le 50°$)	4470 ($3° \le 2\theta \le 44°$)
range of indices	$\pm h, \pm k, +l$	$\pm h, \pm k, +l$
no. of unique reflctns	6821	3913
linear abs coeff, cm^{-1}	6.0	9.6
transmissn factors	N/A	0.83–0.90

(C) Final Model in Least-Squares Refinement

	3	4
final R values[c]	$R_1 = 0.066$, $R_2 = 0.069$	$R_1 = 0.049$, $R_2 = 0.051$
no. of observns	3290 [$F_o \ge 6\sigma(F_o)$]	2692 [$F_o > 4\sigma(F_o)$]
no. of variable parameters	331	375

[a] From a least-squares fit to the setting angles of 25 reflections with $2\theta \ge 23°$ for **3** and $41° \ge 2\theta \ge 17°$ for **4**. [b] By suspension in CCl_4/heptanes for **3** or in CCl_4/benzene for **4**. [c] $R_1 = \sum||F_o| - |F_c||/\sum|F_o|$. $R_2 = [\sum w(|F_o|^2 - |F_c|^2)/\sum w|F_o|^2]^{1/2}$

(sh), 308 (sh), 492 (sh) nm. Anal. Calcd for $Fe_3Cl_3O_7N_{12}C_{54}H_{56}$ ($4 \cdot 2C_6H_6$): C, 51.52; H, 4.48; N, 13.35; Cl, 8.45. Found: C, 51.69; H, 4.58; N, 13.32; Cl, 8.51.

Collection and Reduction of X-ray Data for $[Fe(HTIEO)(TIEO)](ClO_4)_2 \cdot 4H_2O$ ($3 \cdot 4H_2O$). Solvated crystals of approximate dimensions 0.22 × 0.20 × 0.20 mm were mounted in a glass capillary in contact with a small amount of mother liquor to avoid solvent loss. The crystal quality was judged to be acceptable from ω scans of several low-angle reflections ($\Delta\bar{\omega}_{1/2} \approx 0.30$). Study on the diffractometer revealed the crystal to belong to the triclinic Laue class, and a systematic search using TRACER-II[21] failed to reveal higher symmetry. The choice of space group $P\bar{1}$ (C_1^1, No. 2)[22] was confirmed by the solution and refinement of the structure. Data collection and reduction were carried out by previously described procedures,[23] details of which are presented in Table I.

$[Fe_3O(TIEO)_2(O_2CPh)_2Cl_3] \cdot 2C_6H_6$ ($4 \cdot 2C_6H_6$). Yellow crystalline blocks large enough for X-ray diffraction studies were obtained by the slow diffusion of benzene into an acetonitrile solution of **4** over a period of 3–4 weeks. The crystals lose solvent and therefore were flame-sealed in glass capillaries containing a drop of mother liquor. A parallelepiped bounded by (100) and ($\bar{1}00$), 0.225 mm apart, ($10\bar{1}$) and ($\bar{1}01$), 0.175 mm apart, and (110) and ($1\bar{1}0$), 0.150 mm apart, was used for the data collection. Diffractometer data combined with a check for higher symmetry[22] indicated that $4 \cdot 2C_6H_6$ belongs to the triclinic system. The choice of the space group, $P\bar{1}$ (C_1^1, No. 2),[22] was confirmed by a statistical analysis of the data[24] and by the successful solution and refinement of the structure. Data collection and reduction were carried out as previously described,[23] with details summarized in Table I.

Structure Solution and Refinement. $[Fe(HTIEO)(TIEO)](ClO_4)_2 \cdot 4H_2O$ ($3 \cdot 4H_2O$). The structure was solved by direct methods.[24] After the location of the iron atom, which lies in a general position, difference Fourier maps revealed the position of all non-hydrogen atoms and the proton attached to N43. The positions of all the remaining imidazole hydrogen atoms were located from difference Fourier maps, but for these atoms the C–H distances were fixed at 0.95 Å during the refinement. Anisotropic temperature factors were used for the iron atom, atoms in its coordination sphere, three water oxygen atoms, and one ordered perchlorate anion. The second perchlorate group is disordered and was refined as two interpenetrating tetrahedra having a chlorine atom at the geometric center. The oxygen atoms of these groups were assigned half-occupancy factors. The large temperature factors observed for two of the solvent oxygen atoms, O3W and O4W, suggested that these sites may be only partially occupied. The value of the observed density (Table I) also suggested that the number of water molecules in the crystal structure may be slightly overestimated, but this result should be regarded with caution since some H_2O may have been lost during the density measurements. The methyl groups were assigned rotational degrees of freedom and refined as rigid bodies. Hydrogen atoms belonging to H_2O were not located. Neutral atom scattering factors and anomalous dispersion corrections for non-hydrogen atoms were taken from ref 26 and hydrogen atom scattering factors from ref 27. The function minimized during the least-squares refinement[25] was $\sum w(|F_o| - |F_c|)^2$, where either $w = 1.0$ (i.e. unit weights) or $w = 2.5831/[\sigma^2(F_o) + 0.000\,625(F_o)^2]$. A comparison of the two modes of refinement revealed that, in this case, use of a weighting scheme did not lower the estimated standard deviations but increased the values of both R_1 and R_2 (Table I) from 0.0663 and 0.0710 to 0.0683 and 0.0847, respectively, and decreased the quality of the convergence as judged by the overall increase in the parameter shifts. In consequence, the model with unit weights was preferred. The reason for these differences is unknown and was not revealed by an analysis of variance for different classes of reflections in the final refinements using both weighting schemes. The ratios of parameter shift to estimated standard deviation in the final cycle of refinement was 0.5 for the rotational parameters of the methyl group, 0.09 for the thermal parameters of the methyl hydrogen atoms, 0.04 for the oxygen atoms of the disordered perchlorate, and $\leq$0.04 for the rest of the molecule. The largest peak in the final difference Fourier map, ~0.56 e Å^{-3}, was located near one of the perchlorate oxygen atoms. Final positional and thermal parameters are given in Tables II and S1 (supplementary material), respectively. Interatomic distances and angles are presented in Table IV. Positional parameters for hydrogen atoms are given in Table S2. Calculated and observed structure factors are given in Table S3.

$[Fe_3O(TIEO)_2(O_2CPh)_2Cl_3] \cdot 2C_6H_6$ ($4 \cdot 2C_6H_6$). The positions of the three iron atoms were determined by direct methods.[24] All remaining non-hydrogen atoms were located on subsequent difference Fourier maps. The three iron atoms and the atoms bound directly to them were refined anisotropically, while isotropic thermal parameters were assigned to all other atoms.[25] Aromatic rings from benzoate residues and benzene were

(21) Lawton, S. L. *TRACER II, A FORTRAN Lattice Transformation-Cell Reduction Program*; Mobil Oil Corp., Paulsboro, NJ, 1967.
(22) *International Tables for Crystallography*; Hahn, T., Ed.; D. Reidel Publishing Co.: Dordrecht: Holland/Boson, 1983; Vol. A, p 104.
(23) Silverman, L. D.; Dewan, J. C.; Giandomenico, C. M.; Lippard, S. J. *Inorg. Chem.* **1980**, *19*, 3379–3383.
(24) Germain, G.; Main, P.; Woolfson, M. M. *Acta Crystallogr., Sect. A*: **1971**, *A27*, 368–376.
(25) Structure factor calculations and least-squares refinement was carried out with SHELX-76: Sheldrick, G. M. In *Computing in Crystallography*; Schenk, H., Olthof-Hazekamp, R., van Koningsveld, H., Bassi, G. C., Eds.; Delft University: Delft, The Netherlands, 1978; pp 34–42.
(26) *International Tables for X-ray Crystallography*; Kynoch: Birmingham, England, 1974; Vol. IV, pp 99, 149.
(27) Stewart, R. F.; Davidson, E. R.; Simpson, W. T. *J. Chem. Phys.* **1965**, *42*, 3175–3187.

Table II. Final Positional Parameters for $[Fe(TIEO)(HTIEO)](ClO_4)_2 \cdot 4H_2O$ ($3 \cdot 4H_2O$)[a]

atom	x	y	z
Fe	0.59709(12)	0.55232(9)	0.26624(8)
N13	0.4509(6)	0.4212(5)	0.2988(5)
O25	0.7556(5)	0.6665(4)	0.2591(4)
O14	0.5985(5)	0.4455(4)	0.1665(4)
N33	0.5577(6)	0.6608(5)	0.3679(5)
N63	0.4430(7)	0.5642(5)	0.1626(5)
N53	0.7495(7)	0.5525(5)	0.3827(4)
C641	0.3800(8)	0.3877(6)	0.0583(6)
C146	0.4743(8)	0.3629(6)	0.1347(5)
N11	0.3132(7)	0.2604(5)	0.2372(5)
C12	0.4088(8)	0.3444(6)	0.2221(5)
C14	0.3790(9)	0.3829(7)	0.3668(6)
C15	0.2935(9)	0.2844(7)	0.3289(6)
C1M	0.2426(10)	0.1599(7)	0.1715(7)
N41	0.5901(7)	0.2341(5)	0.1383(5)
C42	0.5035(8)	0.2692(6)	0.0917(6)
C4M	0.6611(10)	0.2722(7)	0.2400(7)
N43	0.4588(8)	0.2127(6)	0.0023(5)
C44	0.5195(10)	0.1408(8)	-0.0071(7)
C45	0.6011(10)	0.1542(7)	0.0768(7)
N61	0.2728(7)	0.5156(5)	0.0378(5)
C62	0.3658(8)	0.4879(6)	0.0882(6)
C64	0.3958(9)	0.6438(7)	0.1583(6)
C65	0.2900(9)	0.6129(7)	0.0805(6)
C6M	0.1662(9)	0.4524(7)	-0.0474(6)
N31	0.5922(7)	0.8040(5)	0.4695(5)
C32	0.6502(8)	0.7529(6)	0.4123(6)
C34	0.4356(9)	0.6538(7)	0.3981(6)
C35	0.4569(9)	0.7412(7)	0.4596(6)
C3M	0.6607(10)	0.9084(7)	0.5291(7)
N21	1.0699(7)	0.7254(5)	0.2952(5)
C22	0.9881(8)	0.7760(6)	0.3255(6)
N23	1.0409(8)	0.8735(6)	0.3251(5)
C24	1.1617(11)	0.8864(8)	0.2925(7)
C25	1.1799(10)	0.7971(7)	0.2763(7)
C2M	1.0468(10)	0.6166(7)	0.2827(7)
N51	0.9336(7)	0.6539(5)	0.4921(5)
C52	0.8485(8)	0.6437(6)	0.4072(5)
C54	0.7718(9)	0.5001(7)	0.4522(6)
C55	0.8838(9)	0.5621(7)	0.5188(7)
C5M	1.0582(9)	0.7424(7)	0.5418(7)
C235	0.8486(8)	0.7218(6)	0.3469(6)
C532	0.7945(8)	0.8000(6)	0.3990(6)
O1W	0.0073(9)	0.0639(6)	0.3426(6)
O2W	0.2552(9)	0.2065(6)	-0.1364(5)
O3W	0.874(2)	0.0738(15)	0.9878(17)
O4W	0.927(2)	0.9682(18)	0.1071(14)
C12	0.4085(3)	-0.0067(2)	0.70928(19)
O1C1	0.4511(11)	0.0950(6)	0.6998(7)
O2C1	0.2978(10)	-0.0301(8)	0.7573(8)
O3C1	0.5176(9)	-0.0220(7)	0.7652(7)
O4C1	0.3661(10)	0.9237(7)	0.6189(6)
C11	1.0054(3)	1.3302(2)	0.16672(19)
O5C1	0.9684(3)	1.2639(2)	0.22663(19)
O6C1	1.1327(3)	1.4162(2)	0.21691(19)
O7C1	0.9120(3)	1.3644(2)	0.12934(19)
O8C1	1.0544(3)	1.2795(2)	0.08949(19)
O9C	0.9939(3)	1.3965(2)	0.24357(19)
O10C	0.9778(3)	1.2319(2)	0.18863(19)
O11C	1.1478(3)	1.3671(2)	0.15502(19)
O12C	0.9203(3)	1.3223(2)	0.08263(19)

[a] Atoms are labeled as shown in Figure 3. Estimated standard deviations, in parentheses, occur in the last significant figure(s) for each parameter.

constrained to idealized hexagons; phenyl hydrogen atoms were located on difference Fourier maps and then fixed at a distance of 0.95 Å from the carbon atoms to which they were bound and allowed to ride on them during refinement.[25] A common isotropic temperature factor assigned to these hydrogen atoms was refined to a value of $U = 0.19$ Å^2. The largest residual peak in the final difference Fourier map was 0.79 e Å^{-3}, located near a solvent molecule. The maximum parameter shift was 0.001 σ for the complex and 0.014 σ for one of the solvent carbon atoms in the final cycle of refinement. Again, unit weights were found to be marginally superior to a statistical weighting scheme. Final atomic positional parameters are presented in Table III, final thermal parameters are presented in Table S4, a list of selected bond distances and angles is presented in Table V, hydrogen atom positional parameters are presented in Table S5, and observed and calculated structure factors are presented in Table S6.

Physical Measurements. Mössbauer Spectroscopy. Mössbauer (^{57}Fe) spectra of polycrystalline samples of **4** were recorded at 77 and 4.2 K as described previously.[15] Longitudinal magnetic fields of 60 and 80 kOe were applied at 4.2 K. The isomer shifts were measured relative to iron metal at room temperature.

Mass Spectra. Mass spectra were recorded with a Varian MAT 731 high-resolution mass spectrometer equipped with a field desorption (FD) source and fast atom bombardment (FAB) gun.

Nuclear Magnetic Resonance Spectroscopy. ^{1}H NMR spectra were recorded with Bruker WM 250 and WM 270 spectrometers and are referenced to tetramethylsilane.

Infrared and Optical Spectroscopy. Infrared spectra in the range 400–4000 cm^{-1} were recorded by using Beckman Acculab 10 and Perkin-Elmer Model 283 B instruments at ±5 cm^{-1} accuracy or, for **4**, a Nicolet 7199 Fourier transform instrument. Electronic spectra were recorded in the 250–800-nm range with a Cary Model 118C spectrophotometer.

Magnetic Susceptibility Measurements. Solid-state magnetic measurements of powdered samples of **3** were carried out with an SHE Model 905 SQUID-type susceptometer at 20 kOe. An analytically pure sample

Table III. Final Positional Parameters for $[Fe_3O(TIEO)_2(O_2CPh)_2Cl_3] \cdot 2C_6H_6$ ($4 \cdot 2C_6H_6$)[a]

atom	x	y	z
Fe1	0.49984(12)	0.74000(10)	0.79484(11)
Fe2	0.26855(12)	0.82831(10)	0.91213(11)
Fe3	0.27319(12)	0.81974(10)	0.69719(10)
C11	0.6226(2)	0.6710(2)	0.9276(2)
C12	0.3462(3)	0.8368(2)	1.0675(2)
C13	0.1706(2)	0.85370(19)	0.5490(2)
O3	0.3688(5)	0.7914(4)	0.8316(4)
O2	0.1718(5)	0.8268(4)	0.7826(5)
O1	0.4114(5)	0.8012(4)	0.6633(4)
O4	0.4782(5)	0.6215(4)	0.7542(5)
O5	0.2338(5)	0.9653(4)	0.8823(5)
O6	0.2414(5)	0.9557(4)	0.7232(5)
O7	0.3100(5)	0.6833(4)	0.6815(5)
N11	0.5022(6)	1.0083(5)	0.7948(6)
N13	0.5212(6)	0.8663(5)	0.8159(6)
N21	0.4011(7)	0.7790(6)	0.4508(6)
N23	0.3671(7)	0.9275(6)	0.4518(6)
N31	0.6516(7)	0.7776(6)	0.5842(6)
N33	0.6107(6)	0.7148(5)	0.6986(6)
N41	0.2566(7)	0.5643(6)	0.9066(6)
N43	0.2807(6)	0.6921(5)	0.9265(6)
N51	-0.0417(7)	0.9184(6)	0.6631(6)
N53	-0.0244(7)	0.7750(6)	0.6405(6)
N61	-0.0410(7)	0.8590(6)	0.9115(7)
N63	0.1141(7)	0.8633(5)	0.9474(6)
C12	0.4896(8)	0.9348(7)	0.7517(8)
C14	0.5550(8)	0.8966(7)	0.9035(9)
C15	0.5447(8)	0.9849(7)	0.8917(8)
C16	0.4701(9)	1.1002(7)	0.7553(8)
C22	0.4094(8)	0.8501(7)	0.5032(8)
C24	0.3296(9)	0.9027(8)	0.3629(9)
C25	0.3483(9)	0.8146(8)	0.3600(9)
C26	0.4345(10)	0.6841(8)	0.4820(9)
C32	0.5739(8)	0.7769(7)	0.6270(8)
C34	0.7173(10)	0.6734(8)	0.7006(8)
C35	0.7427(10)	0.7117(8)	0.6300(9)
C36	0.6433(10)	0.8383(8)	0.5047(9)
C42	0.2186(8)	0.6545(7)	0.8783(8)
C44	0.3610(9)	0.6256(7)	0.9863(8)
C45	0.3450(8)	0.5468(8)	0.9735(8)
C46	0.2104(9)	0.4995(8)	0.8692(8)
C52	0.0058(8)	0.8312(7)	0.6982(8)
C54	-0.0932(9)	0.8296(8)	0.5642(9)
C55	-0.1044(9)	0.9169(8)	0.5769(8)
C56	-0.0223(9)	0.0030(8)	0.6985(8)
C62	0.0485(9)	0.8449(7)	0.8777(9)
C64	0.0647(9)	0.8915(7)	1.0265(9)
C65	-0.0301(10)	0.8892(8)	1.0038(9)
C66	-0.1346(11)	0.8497(9)	0.8570(10)
C90	0.4478(8)	0.9352(7)	0.6470(7)
C92	0.4599(8)	0.8413(7)	0.6095(7)
C93	0.1274(8)	0.6960(6)	0.7999(7)
C95	0.0882(8)	0.8017(6)	0.7883(7)
C71	0.3894(5)	0.5238(4)	0.7052(5)
C72	0.4634(5)	0.4505(4)	0.7634(5)
C73	0.4579(5)	0.3645(4)	0.7554(5)
C74	0.3784(5)	0.3520(4)	0.6891(5)
C75	0.3043(5)	0.4253(4)	0.6309(5)
C76	0.3098(5)	0.5113(4)	0.6389(5)
C77	0.3934(10)	0.6160(7)	0.7164(8)
C81	0.2158(5)	1.0956(3)	0.7957(5)
C82	0.2415(5)	1.1390(3)	0.8790(5)
C83	0.2248(5)	1.2314(3)	0.8743(5)
C84	0.1825(5)	1.2803(3)	0.7863(5)
C85	0.1568(5)	1.2369(3)	0.7030(5)
C86	0.1735(5)	1.1445(3)	0.7077(5)
C87	0.2328(8)	0.9970(7)	0.8018(9)
C1S	0.1344(8)	0.7176(7)	0.3353(8)
C2S	0.2078(8)	0.6368(7)	0.3821(8)
C3S	0.2734(8)	0.5692(7)	0.3298(8)
C4S	0.2654(8)	0.5823(7)	0.2307(8)
C5S	0.1919(8)	0.6631(7)	0.1839(8)
C6S	0.1264(8)	0.7308(7)	0.2361(8)
C7S	0.0754(8)	0.4207(6)	0.0482(8)
C8S	0.0053(8)	0.4163(6)	-0.0339(8)
C9S	-0.0691(8)	0.4966(6)	-0.0808(8)
C10S	0.0000(6)	0.5463(5)	0.5845(8)
C11S	0.0255(6)	0.5761(5)	0.5043(8)
C12S	0.0259(6)	0.5289(5)	0.4181(8)

[a] Numbers, in parentheses, are errors in the last significant digit(s). Atoms are labeled as shown in Figure 4. S stands for solvent (benzene). Connectivities are as follows: C77 and C87 are carboxyl carbon atoms; C95 is linked to C52, C62, O2, and C93; C93 bonds to C95 and C42; C92 bonds to C22, C32, O1, and C90; C90 bonds to C92 and C12. The labeling scheme for the phenyl and imidazole rings is

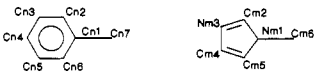

where $n = 7$ and 8 and $m = 1, 2, 3, 4, 5$, and 6.

of $4 \cdot 2C_6H_6$ was used for magnetization studies. It was powdered and dried under vacuum overnight in order to remove the solvent. Intact solvated crystals were used for obtaining variable-temperature susceptibility data, keeping the time of sample manipulation at room temper-

Table IV. Interatomic Distances (Å) and Angles (deg) for $[Fe(TIEO)(HTIEO)](ClO_4)_2 \cdot 4H_2O$ ($3 \cdot 4H_2O$)[a]

Coordination Sphere					
Fe–O25	1.914 (5)	Fe–O14	1.916 (5)	Fe–N63	2.117 (7)
Fe–N33	2.133 (7)	Fe–N13	2.135 (6)	Fe–N53	2.153 (7)
O25–Fe–O14	101.8 (2)	O25–Fe–N63	100.9 (2)	O25–Fe–N33	85.6 (2)
O25–Fe–N13	167.5 (3)	O25–Fe–N53	78.5 (2)	O14–Fe–N63	84.6 (3)
O14–Fe–N33	170.0 (2)	O14–Fe–N13	79.9 (2)	O14–Fe–N53	101.7 (3)
N63–Fe–N33	87.5 (3)	N63–Fe–N13	91.6 (3)	N63–Fe–N53	173.7 (3)
N33–Fe–N13	94.2 (3)	N33–Fe–N53	86.2 (3)	N13–Fe–N53	89.0 (2)
Ligand Geometry					
N11–C12	1.34 (1)	N11–C15	1.37 (1)	N11–C1M	1.46 (1)
C12–N13	1.322 (9)	C12–C146	1.53 (1)	N13–C14	1.38 (1)
C14–C15	1.35 (1)				
N21–C25	1.35 (1)	N21–C22	1.37 (1)	N21–C2M	1.45 (1)
C22–N23	1.30 (1)	C22–C235	1.51 (1)	N23–C24	1.38 (1)
C24–C25	1.33 (2)				
N31–C32	1.35 (1)	N31–C35	1.37 (1)	N31–C3M	1.46 (1)
C32–N33	1.324 (8)	C32–C532	1.49 (1)	N33–C34	1.39 (1)
C34–C35	1.33 (1)				
N41–C42	1.33 (1)	N41–C45	1.37 (1)	N41–C4M	1.47 (1)
C42–N43	1.33 (1)	C42–C146	1.52 (1)	N43–C44	1.37 (2)
C44–C45	1.33 (1)				
N51–C55	1.36 (1)	N51–C52	1.37 (1)	N51–C5M	1.461 (9)
C52–N53	1.309 (9)	C52–C235	1.51 (1)	N53–C54	1.38 (1)
C54–C55	1.34 (1)				
N61–C62	1.34 (1)	N61–C65	1.36 (1)	N61–C6M	1.46 (1)
C62–N63	1.328 (8)	C62–C641	1.48 (1)	N63–C64	1.39 (1)
C64–C65	1.36 (1)				
C146–O14	1.381 (8)	C146–C641	1.54 (1)		
C235–O25	1.408 (8)	C235–C532	1.55 (1)		
H(IM)–N43	0.82 (9)	H(IM)···O2W	1.92 (8)		
C12–N11–C15	107.4 (6)	C12–N11–C1M	128.1 (7)	C15–N11–C1M	124.7 (7)
N13–C12–N11	111.1 (7)	N13–C12–C146	117.9 (6)	N11–C12–C146	131.1 (6)
C12–N13–C14	105.7 (6)	C12–N13–Fe	108.3 (5)	C14–N13–Fe	146.1 (5)
C15–C14–N13	109.2 (8)	C14–C15–N11	106.6 (8)		
C25–N21–C22	106.1 (8)	C25–N21–C2M	125.1 (9)	C22–N21–C2M	128.8 (7)
N23–C22–N21	111.5 (7)	N23–C22–C235	125.2 (9)	N21–C22–C235	123.0 (7)
C22–N23–C24	105.0 (9)	C25–C24–N23	109.8 (9)	C24–C25–N21	108 (1)
C32–N31–C35	107.5 (6)	C32–N31–C3M	126.1 (7)	C35–N31–C3M	126.4 (8)
N33–C32–N31	109.8 (7)	N33–C32–C532	127.2 (8)	N31–C32–C532	122.8 (6)
C32–N33–C34	106.5 (7)	C32–N33–Fe	124.3 (6)	C34–N33–Fe	129.2 (7)
C35–C34–N33	108.7 (7)	C34–C35–N31	107.5 (9)		
C42–N41–C45	109.2 (7)	C42–N41–C4M	126.3 (8)	C45–N41–C4M	124.6 (9)
N43–C42–N41	107.6 (8)	N43–C42–C146	128.1 (8)	N41–C42–C146	124.1 (6)
H(IM)–N43–C42	112 (5)	H(IM)–N43–C44	136 (5)	C42–N43–C44	108.4 (8)
C45–C44–N43	107.9 (9)	C44–C45–N41	107 (1)		
C55–N51–C52	106.2 (6)	C55–N51–C5M	126.4 (8)	C52–N51–C5M	127.3 (7)
N53–C52–N51	110.4 (7)	N53–C52–C235	119.5 (7)	N51–C52–C235	130.0 (6)
C52–N53–C54	106.9 (6)	C52–N53–Fe	108.4 (6)	C54–N53–Fe	143.4 (5)
C55–C54–N53	108.6 (8)	C54–C55–N51	107.9 (8)		
C62–N61–C65	108.5 (6)	C62–N61–C6M	127.1 (8)	C65–N61–C6M	124.4 (8)
N63–C62–N61	110.1 (8)	N63–C62–C641	127.3 (8)	N61–C62–C641	122.5 (6)
C62–N63–C64	106.3 (7)	C62–N63–Fe	123.3 (6)	C64–N63–Fe	130.3 (5)
C65–C64–N63	108.4 (7)	N61–C65–C64	106.7 (9)		
C235–O25–Fe	116.3 (5)	C146–O14–Fe	114.7 (5)		
O14–C146–C42	108.4 (7)	O14–C146–C12	107.5 (5)	O14–C146–C641	109.5 (7)
C42–C146–C12	110.0 (7)	C62–C146–C641	110.4 (6)	C12–C146–C641	111.0 (7)
O25–C235–C22	108.5 (6)	O25–C235–C52	106.2 (5)	O25–C235–C532	109.2 (7)
C22–C235–C52	113.2 (7)	C22–C235–C532	110.9 (6)	C52–C235–C532	108.6 (7)
C32–C532–C235	113.8 (6)	C62–C641–C146	114.2 (6)		
N43–H(IM)···O2W	155 (8)				

Perchlorate Geometry

	min	max	mean
group 1			
Cl–O	1.324 (4)	1.471 (4)	1.405
O–Cl–O	101.3 (2)	117.8 (3)	109.45
group 2			
Cl–O	1.391 (9)	1.41 (1)	1.403
O–Cl–O	107.0 (7)	111.7 (6)	109.45

[a] See footnote *a* of Table II. H(IM) designates the hydrogen atom bound to N43 and O2W, the water molecule hydrogen bonded to it.

ature to a minimum. At the end of the run, this sample was analyzed and shown to have lost solvent corresponding to 10.5% of its original weight. This information was used to adjust the molecular weights employed in subsequent calculations. Raw data were processed in the following manner. Data for the sample container were measured and fit to a polynomial expression in T up to the third power, including a Curie–Weiss term, of the general form given in eq 1. The analytical

$$\chi_{obsd} = \frac{a}{T-b} + c + dT + eT^2 + fT^3 \quad (1)$$

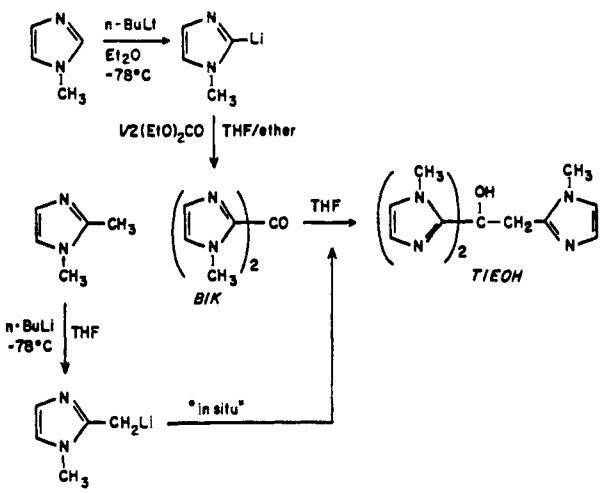

Figure 2. Synthetic routes to polyimidazole ligands.

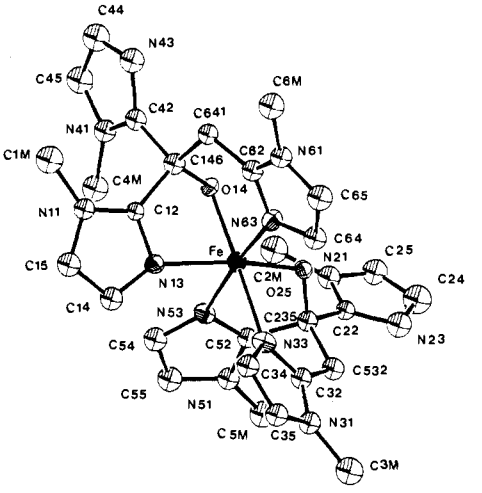

Figure 3. Structure of the cation **3**, showing the 40% probability thermal ellipsoids and the non-hydrogen atom labels. Methyl group carbon atoms are denoted by the letter M.

expression obtained was used to calculate the container susceptibility at any temperature, and, for variable field data, the sample holder was measured at the same field values as the sample. After subtraction of the container values, a diamagnetic correction of -540×10^{-6} cgs units calculated from Pascal's constants was applied.[28] Data at 2.5 and 3.7 K were recorded in fields up to 50 kOe.

Theoretical simulations of the magnetization, M_H, as a function of field were carried out by using the well-known Brillouin function[28c] given in eq 2, with $B_S(y)$ as given in eq 3. In these expressions, S, g, and β

$$M_H = NSg\beta B_S(Sg\beta H/kT) \quad (2)$$

$$B_S(y) = ((2S + 1)/2S) \coth ((2Sy + y)/2S) - (2S)^{-1} \coth (y/2S) \quad (3)$$

are the total spin, the g factor, and the Bohr magneton, respectively, and $y = Sg\beta H/kT$. The ground-state spin was determined from the initial slope. Variable-temperature susceptibility data were collected at 20 kOe between 6 and 296 K. Data processing and experimental and theoretical fits were carried out by using a modified least-squares fitting program.[29] Experimental details and results of the data collection and refinement are presented in Table VI.

Results and Discussion

Synthesis. Although several systematic studies of polyimidazole molecules and their metal complexes have been undertaken,[20,30-33] no iron chemistry has been reported. The synthesis of TIEOH followed the strategy of Breslow et al.[30] for preparing related, expanded ligands (Figure 2). The ketone intermediate (BIK) had been previously reported, but one of the procedures[32] required isolation of an intermediate resulting in overall yields of ~30%, while the other one gave even lower yields and required the use of phosgene.[20] The procedure developed here is a one-pot synthesis that allows the preparation of gram quantities of pure material in high yield. A 50% excess of lithiated imidazole was found empirically to improve both the yield and reproducibility of the results. In the next step the lithiated 1,2-dimethylimidazole reacted smoothly with the ketone. In this case, the use of an excess lithated imidazole did not significantly improve the yield.

The mononuclear complex $[Fe(HTIEO)(TIEO)](ClO_4)_2$ (**3**) was prepared by mixing stoichiometric amounts of ferric perchlorate and the ligand TIEOH. Both ligands have dangling, noncoordinated *N*-methylimidazolyl rings, one of which is protonated (vide infra).

An attempt to synthesize a binuclear (μ-oxo)bis(μ-carboxylato)diiron(III) derivative from $(Et_4N)_2[Fe_2OCl_6]$, sodium benzoate, and TIEOH in acetonitrile led to the formation of small amounts of the trinuclear complex $[Fe_3O(TIEO)(O_2CPh)_2Cl_3]$ (**4**). In order to identify the source of the third iron atom, the stability of $(Et_4N)_2[Fe_2OCl_6]$ in dry, degassed acetonitrile was examined. The Me_4N^+ salt of $[Fe_2OCl_6]^{2-}$ is reported to be unstable in acetonitrile.[34] Repetitive scans of the electronic spectrum of $(Et_4N)_2[Fe_2OCl_6]$ indicated formally 1st order decomposition kinetics with $t_{1/2}$ on the order of 80 min, as monitored by the decrease in intensity of the 293-nm band. Formation of the mononuclear $[FeCl_4]^-$ anion is suggested by an increase in intensity of the 360-nm band and the general appearance of the final spectrum.[17a] Since a clear isosbestic point was lacking, other species are likely to be present in solution, the $\{Fe_3O\}^{7+}$ cation being a likely candidate.

This hypothesis was tested by allowing $\{Fe_2O\}^{4+}$ to react with $[FeCl_4]^-$, as outlined in the Experimental Section, in the presence of sodium benzoate and TIEOH (eq 4-6). The overall reaction

$$(Et_4N)[FeCl_4] + (Et_4N)_2[Fe_2OCl_6] + 2NaO_2CPh \xrightarrow{MeCN} A \quad (4)$$

$$2TIEOH + 2Et_3N \xrightarrow{MeCN} B \quad (5)$$

$$A + B \xrightarrow{MeCN} 4 \xrightarrow{MeCN/C_6H_6} 4{\cdot}2C_6H_6 \quad (6)$$

$$(Et_4N)[FeCl_4] + (Et_4N)_2[Fe_2OCl_6] + 2NaO_2CPh + 2TIEOH + 2Et_3N \rightarrow [Fe_3O(TIEO)_2(O_2CPh)_2Cl_3] + 2NaCl + 3Et_4NCl + 2Et_3NHCl \quad (7)$$

can be formulated as shown in eq 7. This approach was successful, supporting the idea[14] that oxo-bridged polyiron cores can be constructed rationally by starting with the correct ratio of mono- and binuclear reagents (eq 4). The formation of specific products, however, will be favored by the relative amount of carboxylic acid salt present and the choice of added ligand (eq 5). It is conceivable

(28) (a) Earnshaw, A. *Introduction to Magnetochemistry*; Academic: London, 1968. (b) Mulay, L. N. In *Techniques of Chemistry, Volume I, Part IV. Determination of Mass, Transport, and Electrical-Magnetic Properties*; Weissberger, A., Rossiter, B. W., Eds.; Wiley-Interscience: New York, 1972; pp 431-553. (c) van Vleck, J. H. *The Theory of Electric and Magnetic Susceptibilities*; Oxford University: London, 1932; pp 257-259, 316-341.

(29) Karlin, K. Ph.D. Dissertation, Columbia University, 1975.

(30) (a) Tang, C. C.; Davalian, D.; Huang, P.; Breslow, R. *J. Am. Chem. Soc.* **1978**, *100*, 3918-3922. (b) Breslow, R.; Hunt, J. T.; Smiley, R.; Tarnowski, T. *Ibid.* **1983**, *105*, 5337-5342. (c) Tang, C. C. Ph.D. Thesis, Columbia University, New York, 1978.

(31) (a) Slebocka-Tilk, H.; Cocho, J. L.; Frakman, Z.; Brown, R. S. *J. Am. Chem. Soc.* **1984**, *106*, 2421-2431. (b) Brown, R. S.; Salmon, D.; Curtis, N. J.; Dusuma, S. *Ibid.* **1982**, *104*, 3188-3194. (c) Curtis, N. J.; Brown, R. S. *J. Org. Chem.* **1980**, *45*, 4038-4040. (d) Brown, R. S.; Huguet, J. *Can. J. Chem.* **1980**, *58*, 889-901.

(32) Canty, A. J.; George, E. A.; Lee, C. V. *Aust. J. Chem.* **1983**, *36*, 415-418.

(33) (a) Canty, A. J.; Patrick, J. M.; White, A. H. *J. Chem. Soc., Dalton Trans.* **1983**, 1873-1877. (b) Byers, P. K.; Canty, A. J.; Engelhardt, L. M.; Patrick, J. M.; White, A. H. *Ibid.* **1985**, 981-986. (c) Byers, P. K.; Canty, A. J.; Minchin, N. J.; Patrick, J. M.; Skelton, B. W.; White, A. H. *Ibid.* **1985**, 1183-1189.

(34) Neuse, E. W.; Meirim, M. G. *Transition Met. Chem. (Weinheim)* **1984**, *9*, 205-208.

Table V. Interatomic Distances (Å) and Angles (deg) for $[Fe_3O(TIEO)_2(O_2CPh)_2Cl_3]\cdot 2C_6H_6$ ($4\cdot 2C_6H_6$)[a]

Iron Coordination Sphere

Fe1–O3	1.862 (7)	Fe2–O3	1.867 (7)	Fe3–O2	1.992 (7)
Fe1–O4	2.062 (8)	Fe2–O2	2.074 (6)	Fe3–O1	1.994 (7)
Fe1–O1	2.074 (6)	Fe2–O5	2.080 (7)	Fe3–O7	2.034 (7)
Fe1–N13	2.14 (1)	Fe2–N43	2.117 (9)	Fe3–O6	2.057 (7)
Fe1–N33	2.16 (1)	Fe2–N63	2.17 (1)	Fe3–O3	2.067 (6)
Fe1–C11	2.283 (3)	Fe2–C12	2.282 (3)	Fe3–C13	2.264 (3)
O3–Fe1–O4	91.6 (3)	O3–Fe2–O2	81.4 (3)	O2–Fe3–O1	157.0 (2)
O3–Fe1–O1	81.2 (3)	O3–Fe2–O5	91.2 (3)	O2–Fe3–O7	91.0 (3)
O3–Fe1–N13	91.4 (3)	O3–Fe2–N43	90.9 (3)	O2–Fe3–O6	87.5 (3)
O3–Fe1–N33	155.6 (3)	O3–Fe2–N63	155.3 (3)	O2–Fe3–O3	78.7 (3)
O3–Fe1–C11	108.8 (2)	O3–Fe2–C12	109.8 (2)	O2–Fe3–C13	102.5 (2)
O4–Fe1–O1	89.4 (3)	O2–Fe2–O5	88.2 (3)	O1–Fe3–O7	88.3 (3)
O4–Fe1–N13	172.0 (3)	O2–Fe2–N43	83.1 (3)	O1–Fe3–O6	91.5 (3)
O4–Fe1–N33	91.1 (3)	O2–Fe2–N63	74.1 (3)	O1–Fe3–O3	78.3 (3)
O4–Fe1–C11	93.2 (2)	O2–Fe2–C12	168.8 (2)	O1–Fe3–C13	100.5 (2)
O1–Fe1–N13	83.7 (3)	O5–Fe2–N43	170.6 (3)	O7–Fe3–O6	175.9 (2)
O1–Fe1–N33	74.6 (3)	O5–Fe2–N63	90.5 (3)	O7–Fe3–O3	88.8 (3)
O1–Fe1–C11	169.6 (2)	O5–Fe2–C12	92.3 (2)	O7–Fe3–C13	92.3 (2)
N13–Fe1–N33	83.1 (3)	N43–Fe2–N63	83.8 (3)	O6–Fe3–O3	87.1 (3)
N13–Fe1–C11	92.9 (2)	N43–Fe2–C12	95.7 (2)	O6–Fe3–C13	91.7 (2)
N33–Fe1–C11	95.3 (2)	N63–Fe2–C12	94.7 (3)	O3–Fe3–C13	178.3 (3)

Ligand Geometry

O2–C95	1.40 (1)	N21–C26	1.45 (2)	N51–C52	1.35 (1)	C24–C25	1.32 (2)
O1–C92	1.42 (1)	N23–C22	1.32 (1)	N51–C55	1.37 (1)	C32–C92	1.51 (1)
O4–C77	1.25 (2)	N23–C24	1.37 (2)	N51–C56	1.52 (2)	C34–C35	1.35 (2)
O5–C87	1.25 (2)	N31–C32	1.34 (2)	N53–C52	1.32 (2)	C42–C93	1.48 (1)
O6–C87	1.26 (1)	N31–C35	1.37 (1)	N53–C54	1.38 (1)	C44–C45	1.35 (2)
O7–C77	1.27 (1)	N31–C36	1.46 (2)	N61–C62	1.36 (2)	C52–C95	1.51 (1)
N11–C12	1.35 (1)	N33–C32	1.32 (1)	N61–C65	1.37 (2)	C54–C55	1.34 (2)
N11–C15	1.39 (1)	N33–C34	1.38 (1)	N61–C66	1.46 (2)	C62–C95	1.50 (2)
N11–C16	1.45 (1)	N41–C45	1.36 (1)	N63–C62	1.33 (2)	C64–C65	1.33 (2)
N13–C12	1.33 (1)	N41–C42	1.37 (1)	N63–C64	1.38 (2)	C90–C92	1.51 (1)
N13–C14	1.37 (1)	N41–C46	1.45 (2)	C12–C90	1.48 (1)	C93–C95	1.56 (1)
N21–C22	1.35 (1)	N43–C42	1.32 (2)	C14–C15	1.37 (2)		
N21–C25	1.38 (1)	N43–C44	1.38 (1)	C22–C92	1.52 (1)		

Fe1–O3–Fe2	159.1 (3)	C95–O2–Fe3	142.1 (6)	C92–O1–Fe3	142.1 (5)
Fe1–O3–Fe3	100.3 (3)	C95–O2–Fe2	116.6 (6)	C92–O1–Fe1	115.3 (5)
Fe2–O3–Fe3	100.5 (3)	Fe3–O2–Fe2	96.2 (3)	Fe3–O1–Fe1	95.8 (3)
C77–O4–Fe1	126.1 (6)	C87–O5–Fe2	124.7 (7)	C87–O6–Fe3	129.2 (7)
C77–O7–Fe3	129.5 (8)				
C12–N11–C15	107.9 (9)	C12–N13–C14	107.4 (9)	C22–N21–C25	106.2 (9)
C12–N11–C16	129.2 (8)	C12–N13–Fe1	126.7 (7)	C22–N21–C26	128.7 (9)
C15–N11–C16	122.7 (9)	C14–N13–Fe1	125.1 (7)	C25–N21–C26	125 (1)
		C22–N23–C24	103.6 (9)		
C32–N31–C35	107 (1)	C32–N33–C34	106 (1)	C45–N41–C46	126.8 (9)
C32–N31–C36	127.4 (8)	C32–N33–Fe1	111.2 (6)	C42–N41–C46	125.2 (8)
C35–N31–C36	125 (1)	C34–N33–Fe1	139.2 (7)	C45–N41–C42	108 (1)
C42–N43–C44	108.2 (9)	C52–N51–C55	107 (1)		
C42–N43–Fe2	127.4 (6)	C52–N51–C56	129.7 (9)	C52–N53–C54	104.9 (9)
C44–N43–Fe2	124.3 (8)	C55–N51–C56	123.0 (9)		
C62–N61–C65	108 (1)	C62–N63–C64	108 (1)	N13–C12–N11	110.0 (9)
C62–N61–C66	126 (1)	C62–N63–Fe2	113.4 (8)	N13–C12–C90	128 (1)
C65–N61–C66	126 (1)	C64–N63–Fe2	138.4 (8)	N11–C12–C90	122 (1)
C15–C14–N13	109 (1)	C14–C15–N11	106 (1)		
N23–C22–N21	112.1 (9)	C25–C24–N23	112 (1)	C24–C25–N21	106 (1)
N23–C22–C92	124 (1)				
N21–C22–C92	123.5 (9)				
N33–C32–N31	110.9 (8)	C35–C34–N33	109.0 (9)	C34–C35–N31	107 (1)
N33–C32–C92	120 (1)				
N31–C32–C92	129 (1)				
N43–C42–N41	108.7 (8)	C45–C44–N43	108 (1)	C44–C45–N41	107.6 (9)
N43–C42–C93	128 (1)				
N41–C42–C93	123 (1)				
N53–C52–N51	111.4 (9)	C55–C54–N53	111 (1)	C54–C55–N51	106.4 (9)
N53–C52–C95	124.6 (9)				
N51–C52–C95	124 (1)				
N63–C62–N61	108 (1)	C65–C64–N63	108 (1)	C64–C65–N61	108 (1)
N63–C62–C95	118 (1)				
N61–C62–C95	132 (1)				
O1–C92–C32	104.4 (8)	C12–C90–C92	113.6 (8)		
O1–C92–C90	110.1 (8)				
O1–C92–C22	109.7 (9)				
C32–C92–C90	110.6 (9)				
C32–C92–C22	112.7 (8)				
C90–C92–C22	109.3 (8)				

Table V (Continued)

O2–C95–C62	105.2 (9)	C42–C93–C95	114.4 (9)
O2–C95–C52	111.4 (9)		
O2–C95–C93	110.2 (7)		
C62–C95–C52	113.1 (8)		
C62–C95–C93	109.2 (9)		
C52–C95–C93	107.7 (9)		
	Carboxylate Group Atoms		
C77–C71	1.49 (1)	O5–C87–C81	117 (1)
C87–C81	1.49 (1)	O6–C87–C81	115 (1)
O4–C77–O7	125 (1)	O5–C87–O6	127 (1)
O4–C77–C71	118.5 (8)	O6–C87–C81	115 (1)

[a] See footnote *a*, Table III.

Table VI. Experimental Details of the Magnetic Studies of $[Fe_3O(TIEO)_2(O_2CPh)_2Cl_3]\cdot 2C_6H_6$ ($\mathbf{4}\cdot 2C_6H_6$)

(A) Measurement and Treatment of Magnetic Data[a]

	magnetization		var temp suscept
instrument	SQUID	SQUID	SQUID
operation mode	2 K	2 K	normal
temp (K)	2.5	3.7	6–290
field (kOe)	0.5–42.5	0.5–50.0	20
no. of unique data pts[b]	12	10	56
no. of measurements for each pt[c]	10	10	6
μ_{eff}/cluster, μ_B	5.91	5.86	6.5 at 290 K
μ_{eff}/iron, μ_B	3.41	3.38	3.75 at 290 K

(B) Nonlinear Least-Squares Refinement

temp range (K)	16–290
field (kOe)	20
no. of total data points[d]	56
no. of points used for refinement	49
parameters	J_{13}, J_{23}
P[e]	0.00
g[f]	2.00
TIP[g] (cgs mol^{-1})	0.00
J_{12} (cm^{-1})[h]	−55 (1)
J_{13} (cm^{-1})[h]	−8.0 (4)
α[i]	~6.9
correlatn coeff	0.99994
residual factor, R[j]	0.007

[a] Also, see text. [b] Each data point is a (magnetic moment, temperature) pair. [c] Average values are reported. [d] Only points above 16 K were used in refinement. [e] Fraction of a paramagnetic impurity with $S = {}^5/_2$. [f] Landē factor. [g] Temperature-independent paramagnetism. [h] Exchange coupling constants. Note, $J_{13} = J_{23}$, see eq 13. [i] Ratio of J_{12}/J_{13}. [j] $R = \sum|\chi_M^{obsd} - \chi_M^{calcd}|/\sum\chi_M^{obsd}$.

that, under strictly controlled biological conditions, reactions similar to eq 4 take place in vivo during the assembly of the ferritin core.[35] This idea is not inconsistent with the fact that the chemistry shown in eq 4 leads to the known[36,37] polynuclear iron oxo hydroxo complex $[Fe_{11}O_6(OH)_6(O_2CPh)_{15}]$.[17]

Crystals of $\mathbf{4}\cdot 2C_6H_6$ slowly lose solvent when exposed to air. In MeCN solution **4** decomposes slowly over one month. Among the products formed is $[Fe(BIK)_3]Cl_2$, which was isolated in very low yield and structurally characterized.[17] Its formation might occur by oxidation of TIEOH in the presence of oxygen and Fe(III), which is reduced to Fe(II) (eq 8, where R is *N*-

$$R_2C(OH)CH_2R \xrightarrow[O_2]{Fe^{III}} R_2C{=}O + Fe^{II} \rightarrow [Fe(BIK)_3]^{2+} \quad (8)$$

methylimidazol-2-yl). The products of the redox reaction, Fe(II) and bis(*N*-methylimidazol-2-yl)ketone (BIK), combine to form a blue tris-chelate complex. Removal of $[Fe(BIK)_3]Cl_2$ can be accomplished by washing the crude product with a 1:7 v/v mixture of benzene/acetonitrile to leave pure crystals of $\mathbf{4}\cdot 2C_6H_6$.

Description of the Structures. Mononuclear $[Fe(HTIEO)(TIEO)]^{2+}$ (3). The structure of cation **3** is displayed in Figure 3. The iron coordination sphere is distorted octahedral with two imidazole nitrogen atoms and one alkoxide oxygen atom contributed by each of two facially coordinating ligands bound to the metal center. The two oxygen atoms are cis to one another in the coordination sphere. The geometry of the resulting FeN_4O_2 inner coordination shell, with average Fe–N and Fe–O bond lengths of 2.135 and 1.915 Å, respectively, is quite similar to that of six-coordinate iron(III) complexes with hexadentate ligands derived from condensing triethylenetetramine with β-diketones or salicylaldehyde.[38] This similarity suggests that imine- and amine-type nitrogen atoms are reasonable geometric mimics of the biologically more relevant imidazole-type nitrogen atoms. The values of the angles at iron in **3** increase toward 90° with the size of the chelate ring, being 79° for the five-membered O–Fe–N ring, 85° for the six-membered O–Fe–N ring, and 89° for the seven-membered N–Fe–N ring. Further structural details are given in Table IV.

One of the dangling imidazole rings in **3** is protonated, specifically, at nitrogen atom N43 (Figure 3). Evidence for the existence of a proton at this position comes from the location and successful refinement of the hydrogen atom in the crystal structure analysis, from the slightly expanded internal C–N–C angle at nitrogen N43 compared to all the other unmethylated imidazole ring nitrogens in the complex,[39] and from the overall 2+ charge on the complex, which is balanced by two perchlorate anions. This proton is hydrogen bonded to water oxygen atom O2W in the lattice, the N43···O2W distance being 2.69 (2) Å. The other noncoordinated imidazole nitrogen atom, N23, forms a hydrogen bond, this time as an acceptor, with water molecule O1W, at a N23···O1W distance of 2.82 (1) Å. Water molecules O3W and O4W are linked via hydrogen bonds to their symmetry related counterparts O3W′ and O4W′, forming a rhombus with the sides O3W···O4W′ = 2.82 (4) Å and O3W···O4W = 2.57 (4) Å. This unit of four water molecules is further hydrogen-bonded to water molecules O2W and O2W′.

Trinuclear $[Fe_3O(TIEO)_2(O_2CPh)_2Cl_3]$ (4). Figure 4 depicts the entire structure of **4**, while Figure 5 highlights the coordination spheres of the three iron atoms. These three atoms define an isosceles triangle, and the μ_3-oxo atom O3 is displaced by only 0.04 Å from the plane of this triangle. Each iron atom has pseudooctahedral symmetry, with two nitrogen, three oxygen, and one chlorine atom in the coordination spheres of the equivalent Fe1 and Fe2 atoms. Five oxygen and one chlorine atom constitute the coordination sphere of the unique Fe3 atom. The potentially tetradentate ligand $TIEO^-$ is only tridentate, binding to iron through its deprotonated alkoxo oxygen, unique imidazole nitrogen, and only one of the two equivalent imidazole nitrogen atoms. These some three moieties are bound to iron in the mononuclear

(35) (a) Ford, G. C.; Harrison, P. M.; Rice, D. W.; Smith, J. M. A.; Treffry, A.; White, J. L.; Yariv, J. *Phil. Trans. R. Soc. Lond. B* **1984**, *304*, 551–564. (b) *ibidem*, *Rev. Port. Quim.* **1985**, *27*, 119–120. (c) Spiro, T. G.; Saltman, P. *Struct. Bonding (Berlin)* **1969**, *6*, 116–156. (d) Spiro, T. G.; Pope, L.; Saltman, P. *J. Am. Chem. Soc.* **1967**, *89*, 5555–5559. (e) Spiro, T. G.; Bates, G.; Saltman, P. *J. Am. Chem. Soc.* **1967**, *89*, 5559–5562. (f) Theil, E. C. *Adv. Inorg. Biochem.* **1983**, *58* 1–38 and references cited therein.
(36) Gorun, S. M.; Lippard, S. J. *Nature (London)* **1986**, *319*, 666–667.
(37) Lippard, S. J. *Chem. Br.* **1986**, 222–229.
(38) Sinn, E.; Sim, G.; Dose, E. V.; Tweedle, M. F.; Wilson, L. J. *J. Am. Chem. Soc.* **1978**, *100*, 3375–3390.
(39) Cf. Heitner, H. I.; Lippard, S. J. *Inorg. Chem.* **1974**, *13*, 815–822.

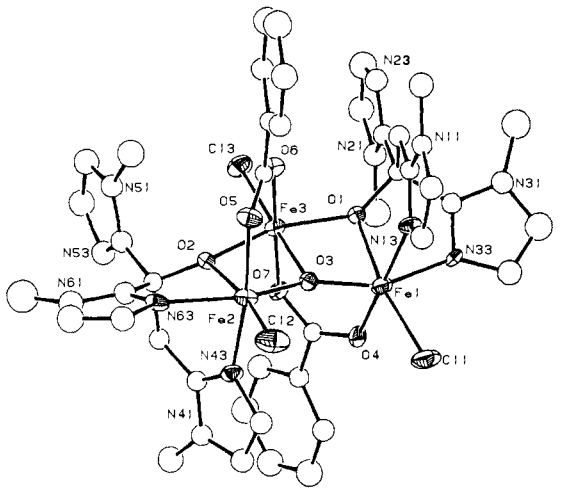

Figure 4. Structure of **4**, showing the 40% probability thermal ellipsoids and labels for all non-hydrogen atoms except carbon.

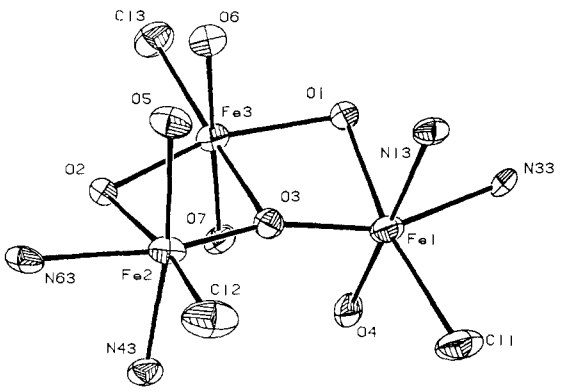

Figure 5. Structure of the iron coordination spheres of **4**, showing the 40% probability thermal ellipsoids.

$[Fe(HTIEO)(TIEO)]^{2+}$ complex **3**. The difference is that, in **4**, the alkoxide groups bridge the Fe1···Fe3 and Fe2···Fe3 iron atom pairs along the equivalent sides of the triangle, whereas in the mononuclear complex the alkoxide groups are terminal. Each of the two alkoxo-bridged diiron pairs in **4** is also bridged by a bidentate benzoate ligand. The coordination spheres of the equivalent iron atoms are completed by two imidazole nitrogen atoms and one chloride ion. A third chloride, trans to the μ_3-oxo atom, completes the coordination sphere of the unique Fe3 atom. The two equivalent parts of the core can be related by an approximate twofold symmetry axis passing through O3···Fe3···C13 atoms (Figure 5). The metal–ligand bond distances (Table V) are typical of those found in high-spin mono-, bi- and polynuclear iron(III) complexes (see ref 10, 15, 36, and 38).

There are four benzene molecules per unit cell, two of which are located in general positions and two on inversion centers. The presence of these solvent molecules in the lattice is further corroborated by the elemental analysis of the intact crystals and by their density.

The most important structural feature of **4** is the asymmetry of the $\{Fe_3O\}^{7+}$ core, which is unique among the structurally characterized (μ_3-oxo)triiron(III) complexes.[10] The metal–metal distances are Fe1···Fe3, 3.018 (1) Å, and Fe2···Fe3, 3.027 (1) Å, along equivalent sides of the isosceles triangle and 3.667(1) Å along the inequivalent one. The Fe–Cl distances reflect the asymmetry of the core, the Fe3–C113 distance, 2.264 (3) Å, being somewhat shorter than Fe1–C111, 2.283 (3) Å, and Fe2–C112, 2.282 (3) Å. The geometry of the $TIEO^-$ ligand is normal and compares favorably with that in the mononuclear complex discussed above (Table V). The benzoate geometry is also unremarkable.

Electronic, Vibrational, and NMR Spectra. Mononuclear $[Fe(HTIEO)(TIEO)]^{2+}$ (3). The pale yellow color of high-spin **3**, the optical spectrum of which consists of a peak at 343 nm and a shoulder at 476 nm, contrasts with the dark red color of its low-spin analogues.[17] Similarly, the ^1H NMR spectrum, recorded in the −70 to +70 ppm range, exhibits broad unresolved resonances extending upfield to −30 ppm and sharper peaks that may be assigned to uncoordinated imidazole rings, in accord with the solid-state structure.

Trinuclear $[Fe_3O(TIEO)_2(O_2CPh)_2Cl_3]$ (4). Symmetric (300 cm^{-1}) and asymmetric (600 cm^{-1}) Fe–O stretching frequencies associated with the $\{Fe_3O\}^{7+}$ core in $[Fe_3O(O_2CCH_3)_6(py)_3]^+$ have recently been assigned with the aid of isotopic substitution.[40] In C_{2v} symmetry there are six bands expected for the $\{Fe_3O\}^{7+}$ core, all of them both IR and Raman active. Without isotopic substitutions, little progress can be made in assigning the vibrational spectrum of **4**. Similarly, the electronic spectrum of this trinuclear complex is not very informative, consisting of several shoulders on an intense tail extending from the ultraviolet into the visible region. This spectrum contrasts markedly with those of the more symmetric basic iron carboxylates, however, in which the charge-transfer bands extend further into the visible.[8a,41,42] On the basis of electronic spectroscopy, **4** seems to be an intermediate case between a binuclear $\{Fe_2O\}^{4+}$ and symmetric trinuclear $\{Fe_3O\}^{7+}$ complex, in accord with its magnetic behavior (see below). Further insight must await detailed calculations and further experimental studies of the electronic structure of **4**.

Magnetochemistry. The room-temperature magnetic moment, 6.0 μ_B, of a solid sample of **3** is consistent with high-spin iron(III). The rest of this section is devoted to an analysis of the magnetic properties of the trinuclear complex **4**.

Magnetization Studies. Assignment of the Ground State of $[Fe_3O(TIEO)_2(O_2CPh)_2Cl_3]$. In principle, the ground state of a molecule with three high-spin iron(III) atoms can have any total spin value, S_T, between $^1/_2$ and $^{15}/_2$. In a simple vectorial coupling model S_T is defined by eq 9, where the subscripts 1, 2, and 3 denote

$$\vec{S}_T = \vec{S}_1 + \vec{S}_2 + \vec{S}_3 \tag{9}$$

the three $S = {}^5/_2$ centers. Coupling two centers to give a partial spin, S_p, results in expressions 10 and 11. Assuming isotropic

$$\vec{S}_p = \vec{S}_1 + \vec{S}_2,\ |\vec{S}_p| = |\vec{S}_1 - \vec{S}_2|,\ |\vec{S}_1 - \vec{S}_2 + 1|,\ \ldots,\ |\vec{S}_1 + \vec{S}_2| \tag{10}$$

$$\vec{S}_T = \vec{S}_p + \vec{S}_3,\ |\vec{S}_T| = |\vec{S}_p - \vec{S}_3|,\ |\vec{S}_p - \vec{S}_3 + 1|,\ \ldots,\ |\vec{S}_p + \vec{S}_3| \tag{11}$$

exchange, the spin Hamiltonian can be written as in eq 12, where

$$H = -2 \sum_{i>j=1}^{3} J_{ij}\vec{S}_i\cdot\vec{S}_j \tag{12}$$

J_{ij} are the exchange coupling constants between the i,j pairs. Since the Fe···Fe distances are longer than 3 Å (vide supra), superexchange through bridging ligands is expected to be the major mechanism for spin coupling.

In the classical case of the basic iron acetates of D_{3h} symmetry, where the ground state has $S_T = {}^1/_2$, all three exchange couplings were initially assumed to be equal, based on limited magnetic data.[43] The use of inequivalent exchange interactions was subsequently introduced to explain the magnetic behavior of these compounds over an extended temperature range.[41,43-46] In com-

(40) Montri, L.; Canon, R. D. *Spectrochimica Acta, Part A* **1985**, *41A*, 643–646.
(41) Long, G. J.; Robinson, W. T.; Tappmeyer, W. P.; Bridges, D. L. *J. Chem. Soc., Dalton Trans.* **1973**, 573–579.
(42) Dubicki, L.; Martin, R. L. *Aust. J. Chem.* **1969**, *22*, 701–705.
(43) Kambe, K. J. *Phys. Soc. Jpn.* **1950**, *5*, 48–51.
(44) (a) Abragam, A.; Horowitz, J.; Yvon, J. *J. Phys. Radium* **1952**, *13*, 489–490. (b) Yvon, J.; Horowitz, J.; Abragam, A. *Rev. Mod. Phys.* **1953**, *25*, 165. (c) Föex, G.; Tsai, B.; Wucher, *J. Compt. Rend.* **1951**, *233*, 1431–1433.
(45) Duncan, J. F.; Kanekar, C. R.; Mok, K. F. *J. Chem. Soc. A* **1969**, 480–482.
(46) Martin, R. L. In *New Pathways in Inorganic Chemistry*; Ebsworth, E. A. V., Maddock, A., Sharpe, A. G., Eds.; Cambridge University: London, 1968; pp 175–231 and references cited therein.

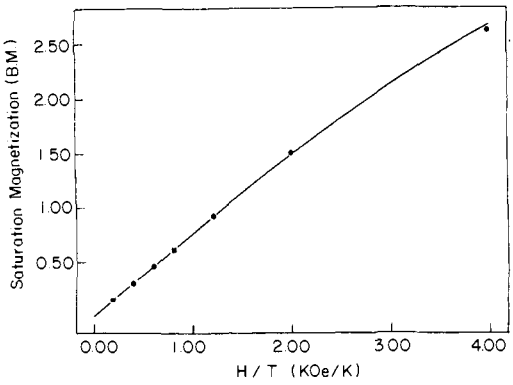

Figure 6. Experimental (points) magnetic moments of **4** at 2.5 K as a function of H/T for magnetic fields up to 10 kOe. The solid line gives the theoretical Brillouin curve for $S_T = {}^5/_2$.

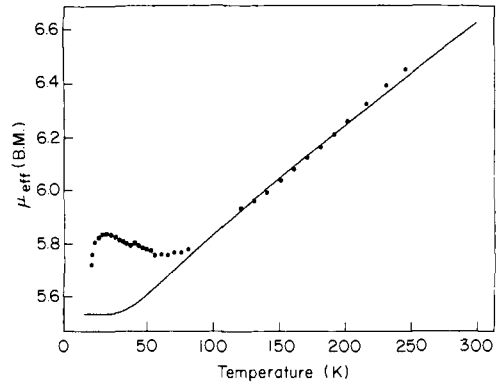

Figure 7. Plot of the experimental and calculated (case I, eq 15—see text) effective magnetic moment for **4** as a function of temperature.

pound **4**, however, the symmetry of the $\{Fe_3O\}^{7+}$ core is approximately C_{2v}. Magnetization data at 2.5 K (Figure 6) and at 3.5 K (data not shown) for fields up to 10 kOe are simulated very well by the Brillouin curve for $S_T = {}^5/_2$. The full value of 5 μ_B for the saturation magnetization was not reached at high H/T (data not shown), possibly due to zero field splitting (see below).

For C_{2v} symmetry, the situation represented by the Hamiltonian of eq 12 may be depicted by the following scheme (eq 13). If

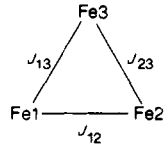

(13)

we consider the exchange integrals to be equal along equivalent sides of the isosceles triangle in **4**, then

$$|J_{13}| = |J_{23}| < |J_{12}| \tag{14}$$

The inequality in eq 14 expresses the expectation that the more remote Fe3 will be less strongly coupled to Fe1 and Fe2 than the latter two are with each other. With only two J values to consider, the ground-state energy can be calculated as a function of the ratio J_{12}/J_{13}. Partial spin state correlation diagrams previously computed for d^5 ions[46,47] were extended for our case with the result that, for $|J_{12}|/|J_{13}| \geq 3.5$, the ground state is predicted to be $|S_T = {}^5/_2, S_p = 0\rangle$. This situation may be compared to the linear case:

$$\text{Fe1—Fe3—Fe2}$$

for which $|S_T = {}^5/_2, S_p = 5\rangle$ because two strong antiferromagnetic (AF) interactions occur between pairs of iron atoms Fe1···Fe3 and Fe2···Fe3.[47d] The difference between the $|S_T = {}^5/_2, S_p = 0\rangle$ and $|S_T = {}^5/_2, S_p = 5\rangle$ ground states is also manifest in the Mössbauer spectra (see below).

Magnetic Susceptibility Studies. Variable-temperature magnetic susceptibility studies were carried out in order to determine the spin exchange coupling constants in **4**. Two cases for which $S_T = {}^5/_2$ were considered, one in which there is no coupling between Fe1···Fe3 and Fe2···Fe3 iron atom pairs, i.e. $|J_{12}| \neq 0$ and $|J_{13}| = |J_{23}| = 0$ (case 1), and one where $|J_{13}| = |J_{23}| \neq 0$ but weak enough to preserve the $|S_T = 5/2, S_p = 0\rangle$ ground state. Since the ordering of the magnetic energy levels is different for the two cases, it was possible to distinguish them by analyzing the temperature dependence of the magnetic data.

Case 1. In this case the system behaves like the sum of an antiferromagnetically coupled, binuclear iron(III) center, comprised of Fe1 and Fe2 and an independent paramagnetic center, Fe3. From the Heisenberg–Dirac–van Vleck theory,[28c] the expression for the molar susceptibility, χ_M,[48a] can be given by eq 15, where $x = J_{12}/kT$, TIP is the temperature-independent

$$\chi_M = \frac{2Ng^2\beta^2}{kT}\,\frac{e^{2x} + 5e^{6x} + 14e^{12x} + 30e^{20x} + 55e^{30x}}{1 + 3e^{2x} + 5e^{6x} + 7e^{12x} + 9e^{20x} + 11e^{30x}} + \text{TIP} + p\frac{4.38}{T} \tag{15}$$

paramagnetism, g is the g factor, and p is the relative amount of the isolated paramagnetic center with $S = {}^5/_2$. TIP and g were fixed to 0.0 and 2.00, respectively. Least-squares fits of the observed data to eq 15 are presented in Figure 7 as a plot of μ_{eff} vs T. Data above 100 K give $J_{12} = -57$ cm^{-1} and $p = 0.9$ instead of 1.0 as expected from the molecular formula. These results, combined with the poor fit (Figure 7) at lower temperatures, indicate that one cannot assume Fe3 to be magnetically independent of the binuclear Fe1···Fe2 center.

Case 2. The Hamiltonian in eq 12 may be rewritten as shown in eq 16. The first part of the equation represents the isotropic

$$H = -2[J_{13}(\vec{S}_1\cdot\vec{S}_2 + \vec{S}_1\cdot\vec{S}_3 + \vec{S}_2\cdot\vec{S}_3) + (J_{12} - J_{13})\vec{S}_1\cdot\vec{S}_2] \tag{16}$$

Hamiltonian (eq 12) for the undistorted (D_{3h}) equilateral triangle of three metals with equivalent exchange couplings, J_{13}, while the second part is the supplementary interaction between Fe1 and Fe2 induced by geometric distortion toward a C_{2v} isosceles triangle.

While in D_{3h} symmetry the energy, $E°$, is a function only of S_T, in C_{2v}, it depends both upon S_T and S_p. The energy, $E(S_T, S_p)$, of the $|S_T, S_p\rangle$ state of the C_{2v} cluster in zero field is given by eq 17, where $E°(S_T) = -J_{13}[S_T(S_T + 1) - 3(35/4)]$,[43] and the

$$E(S_T,S_p) = E°(S_T)—(J_{12} - J_{13})[S_p(S_p + 1)—35/2] \tag{17}$$

expression for the molar susceptibility becomes eq 18. Simple

$$\chi_M = \frac{Ng^2\beta^2}{3kT}\,\frac{\sum_{S_T}\sum_{S_p} S_T(S_T + 1)(2S_T + 1)\exp[-E(S_T,S_p)/kT]}{\sum_{S_T}\sum_{S_p}(2S_T + 1)\exp[-E(S_T,S_p)/kT]} \tag{18}$$

algebraic manipulation of eq 17 and 18 gives the analytical expression[48b] for $\chi_M(J_{12},J_{13},T)$:

$$\chi_M = \frac{Ng^2\beta^2}{4kT}\,\frac{F}{G} \tag{19}$$

where

$$F = F_2 + F_3 + 10x^3(F_T - F_5) + 35x^8(1 + F_T) + 84x^{15}F_T + 165x^{24}(F_T - F_1) + 286x^{35}(F_3 + F_4 + F_5) + 455x^{48}(F_4 + F_5) + 680x^{63}F_5$$

(47) (a) Gayda, J.-P.; Bertrand, P.; Theodule, F.-X.; Moura, J. J. G. *J. Chem. Phys.* **1982**, *77*, 3387–3391. (b) Kent, T. A.; Huynh, B. H.; Münck, E. *Proc. Natl. Acad. Sci. U.S.A.* **1980**, *77*, 6574–6576. (c) Griffith, J. S. *Struct. Bonding (Berlin)* **1972**, *10*, 87–126. (d) Girerd, J.-J.; Papaefthymiou, G. C.; Watson, A. D.; Garup, E.; Hagen, K. S.; Edelstein, N.; Frankel, R. B.; Holm, R. H. *J. Am. Chem. Soc.* **1984**, *106*, 5941–5947 and references cited therein.

(48) (a) See: O'Connor, C. J. *Prog. Inorg. Chem.* **1982**, *29*, 204–283. The paramagnetic impurity was introduced in a different way in eq 15. (b) See also: Kakos, G. A.; Winter, C. *Aust. J. Chem.* **1969**, *22*, 97–101.

$$G = F_2 + F_3 + 2x^3(F_T - F_5) + 3x^8(1 + F_T) + 4x^{15}F_T + 5x^{24}(F_T - F_1) + 6x^{35}(F_3 + F_4 + F_5) + 7x^{48}(F_4 + F_5) + 8x^{63}F_5$$

$$F_1 = y^2 \quad F_2 = y^6 \quad F_3 = y^{12} \quad F_4 = y^{20}$$

$$F_5 = y^{30} \quad F_T = \sum_{i=1}^{5} F_i \quad x = \exp(J_{13}/kT) \quad y = \exp[(J_{12} - J_{13})/kT] \qquad (20)$$

Figure 8 displays the fit of the data above 16 K to this expression, Table VI gives the numerical results of the refinement, and the observed and calculated magnetic susceptibilities are listed in Table S7. There was no need to introduce paramagnetic impurity or TIP correction terms, and the agreement is considered to be very good. Owing mainly to saturation and possibly a small zero field splitting (ZFS) contribution, the magnetic moment deviates from the theoretical curve below 16 K. At 0 K the theoretical effective moment vs. T curve of Figure 8 extrapolates to $\mu_{eff} = 5.92\ \mu_B$, as predicted from the $|S_T = {}^5/_2, S_p = 0\rangle$ ground state.

It is interesting to note the minimum in μ_{eff} at ~60 K, a result that can be readily understood if one considers the ordering of states just above the ground state. From eq 17 and the values of the exchange coupling constants in Table VI, we compute the first excited state to be $|S_T = {}^3/_2, S_p = 1\rangle$, which lies 54 cm^{-1} above the ground state. Since the total spin of the state is ${}^3/_2$, its population reduces the effective moment of the complex. Population of higher energy levels with $S_T \geq {}^5/_2$ occurs above 60 K, which accounts for the increase in μ_{eff} at higher temperatures. In case 1, considered above, μ_{eff} increases monotonically (Figure 7) because the moments of the $S = {}^5/_2$ and spin-coupled binuclear centers simply add.

The J_{12} value of −55 (1) cm^{-1} between iron centers Fe1 and Fe2 connected by a bridging oxygen atom with Fe–O bond lengths of 1.862 (7) Å may be compared with J values of −121 (1) cm^{-1} for the (μ-oxo)diiron(III) center in $[Fe_2O(O_2CCH_3)_2(HBpz_3)_2]$, $(Fe-O)_{av}$ distance of 1.784 (4) Å,[15] and $J = -17$ cm^{-1} in $[Fe_2(OH)(O_2CCH_3)_2(HBpz_3)_2^+$, $(Fe-O)_{av}$ distance of 1.956 (4) Å.[16a] Metalation of the μ-oxo bridge increases the μ-oxo–iron bond length and diminishes the antiferromagnetic exchange coupling constant in a manner similar to protonation of the bridge, but to a lesser degree. It is interesting that the value of the antiferromagnetic coupling constant J correlates with the length of the Fe–O bridge bonds in these polynuclear iron(III) oxo aggregates.[17b] Thus, the longest μ-oxo bridge bond length in **4**, Fe3–O3 = 2.067 (6) Å, occurs along the short edges of the isosceles triangle for which $J_{13} = -8.0$ (4) cm^{-1}. The occurrence of alkoxide bridges along these edges complicates the situation, however. Finally, it may be noted that the observed ratio $|J_{12}|/|J_{13}|$ is ~7, consistent with the $|S_T = {}^5/_2, S_p = 0\rangle$ ground state as predicted above.

Mössbauer Spectroscopy. Experimental results and simulated spectra are presented in Figures 9 and 10. The ^{57}Fe Mössbauer spectrum at 77 K consists of a slightly asymmetric doublet (Figure 9a). A least-squares fit (solid line) to the experimental points, assuming a Lorentzian line shape, gives an isomer shift, $\delta = 0.43$ mm/s, within the range of 0.3 to 0.6 mm/s typically observed for high-spin iron(III) complexes.[49,50] The quadrupole splitting, $\Delta E_Q = 0.86$ mm/s, is outside the 1.5–2.0 mm/s range observed for oxo-bridged complexes[50] and higher than the 0.45–0.71 mm/s range found for basic iron carboxylates.[41] At 4.2 K, the asymmetry is more obvious and a fit with two sets of parameters gives the results: $\delta_1 = 0.48$ and $\delta_2 = 0.52$ mm/s; $\Delta E_{Q1} = 1.16$ and $\Delta E_{Q2} = 0.74$ mm/s.

The Mössbauer spectrum in a longitudinal magnetic field, $H_0 = 60$ kOe, is shown in Figure 10. The spectrum can be decomposed into two magnetic subsites with relative intensities 2:1. The more intense subsite, corresponding to Fe1 and Fe2, has a total magnetic field at the nucleus $|\vec{H}_n| = 60$ kOe. The less intense

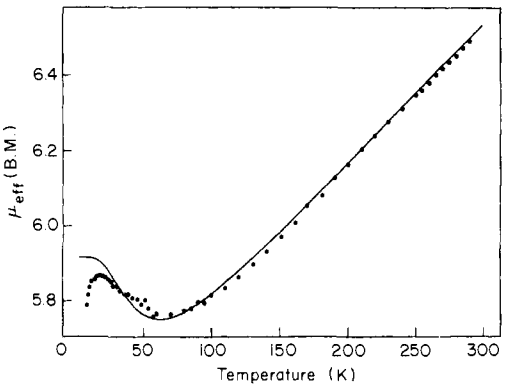

Figure 8. Plot of the experimental and calculated (case II, eq 21—see text) effective magnetic moment of **4** as a function of temperature.

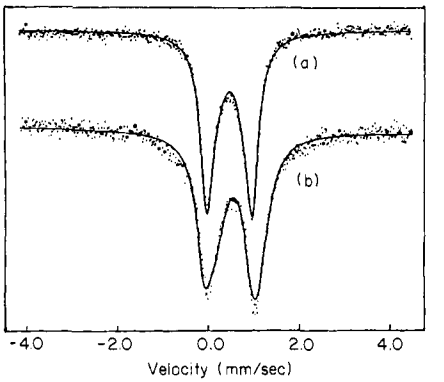

Figure 9. Zero-field Mössbauer spectra of **4** at 77 (a) and 4.2 K (b). The solid lines are least-squares fit to the data.

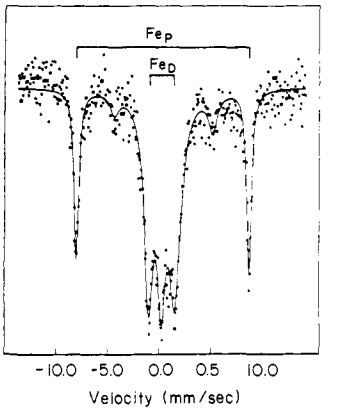

Figure 10. Magnetic Mössbauer spectra of **4** at 4.2 K and $H_0 = 60$ kOe applied parallel to the γ-ray direction. The overbars designate splitting of the outermost absorption lines of the diamagnetic (Fe_D, Fe1 and Fe2) and paramagnetic (Fe_P, Fe3) iron sites. The solid line represents a least-squares fit of the experimental data to Lorentzian lines.

subsite, corresponding to Fe3, has $|\vec{H}_n| = 480$ kOe. The values of $|\vec{H}_n(1,2)|$ and $|\vec{H}_n(3)|$ increase and decrease, respectively, with increasing applied field. Since

$$\vec{H}_n(i) = \vec{H}_{hf}(i) + \vec{H}_0 \qquad (21)$$

where $\vec{H}_{hf}(i)$ is the magnetic hyperfine field at the ith site, these results give $\vec{H}_{hf}(1,2) = 0$ kOe and $\vec{H}_{hf}(3) = -540$ kOe.

These magnetic hyperfine fields are consistent with the $|S_T = {}^5/_2, S_p = 0\rangle$ ground state of the complex. The magnetic hyperfine field at the ith site in an external magnetic field is proportional to the projection of the local spin $\langle S_{iz}\rangle$ on the magnetic field direction (eq 22) where a_i is the magnetic hypefine coupling

$$\vec{H}_{hf}(i) = -\frac{a_i\langle\vec{S}_{iz}\rangle}{g_n\beta_n} \qquad (22)$$

constant, g_n is the nuclear g factor, and β_n is the nuclear magneton.

(49) Greenwood, N. N.; Gibb, T. C. *Mössbauer Spectroscopy*; Chapman and Hall, Ltd.: London, 1971; pp 148–164.
(50) Murray, K. S. *Coord Chem. Rev.* **1974**, *12*, 1–35.

For high-spin iron(III), $a_i/g_n\beta_n \approx -220$ kOe/spin. At large values of H_0/T, the projection of the total spin on the magnetic field, $\langle S_{Tz}\rangle$, approaches $^5/_2$. For the $|S_T = {}^5/_2, S_{Tz} = {}^5/_2\rangle$ substate, $S_{1z} = S_{2z} = 0$ and $S_{3z} = {}^5/_2$. Therefore, from eq 22, $\tilde{H}_{hf}(1) = \tilde{H}_{hf}(2) = 0$ kOe and $\tilde{H}_{hf}(3) = -550$ kOe, in good agreement with the experiment. By comparison, the linear $[Fe_3S_4]^+$ cluster referred to above[47d] has an $|S_T = {}^5/_2, S_p = 5\rangle$ ground state. In this case, all the $\langle S_{iz}\rangle$ values in the $\langle S_{Tz} = {}^5/_2\rangle$ sub-level are nonzero, resulting in two magnetic subsites with 2:1 intensity ratio and nonzero magnetic hyperfine fields of opposite sign.

Weak $\Delta m = 0$ lines observed at $\sim$5 and -4 mm/s in Figure 10 indicate a small zero field splitting of the ground state of the cluster. This finding may partly explain the previously noted disagreement between the observed and calculated susceptibilities at very low temperatures (Figure 8 and Table S7).

Conclusions. A new polyimidazole ligand, TIEOH, has been synthesized and characterized. Such ligands are destined to play an increasingly important role as bioinorganic chemists strive to mimic and elucidate the physical and chemical properties of metal centers in biology.[51] The asymmetric core of the μ_3-oxo complex $[Fe_3O(TIEO)_2(O_2CPh)_2Cl_3]$ represents a topological isomer of symmetric $\{Fe_3O\}^{7+}$ units found in basic iron acetates and their analogues. The different ground states elucidated here correlate with the different geometries. Knowledge of the structural and magnetic properties of these trinuclear clusters is fundamental to understanding larger iron-oxo aggregates in which these Fe_3O units may be viewed as fundamental building blocks.[8,17,36,37] In future papers we shall describe $\{Fe_4O_2\}^{8+}$ and $\{Fe_{11}O_6(OH)_6\}^{15+}$ (see also ref 36) cores that illustrate this principle.

Acknowledgment. This work was supported by National Institutes of Health Research Grant GM 32134 (to S.J.L.) from the National Institute of General Medical Services. Some of the mass spectra were provided by the Facility supported by NIH Grant RR 00317 (Principal Investigator Professor K. Biemann) from the Biotechnology Resources Branch, Division of Research Resources. R.B.F. and G.C.P. were supported by the Office of Naval Research. The Francis Bitter National Magnet Laboratory is supported by the National Science Foundation.

Supplementary Material Available: Tables S1-S7 reporting thermal parameters, and hydrogen atom parameters for $3{\cdot}4H_2O$ and $4{\cdot}2C_6H_6$ and magnetic data for the latter compound (6 pages); tables of structure factors for $3{\cdot}4H_2O$ and $4{\cdot}2C_6H_6$ (26 pages). Ordering information is given on any current masthead page.

(51) For a recent example, see: Sorrell, T. N.; Borovik, A. S. *J. Am. Chem. Soc.* **1986**, *108*, 2479-2481. In this work the Ag(I) and Cu(I) complexes of tris[2-(1-methylimidazolyl)]methoxymethane are reported. We have independently prepared this ligand and studied its chemistry with ferric salts.[17]

Synthesis, Structure, and Spectroscopic Properties of an Unusual Copper(I) Dimer Having Imidazole Ligands. A Model for the Carbonyl Derivative of Hemocyanin and Implications for the Structure of Deoxyhemocyanin

Thomas N. Sorrell*[1] and A. S. Borovik

Contribution from the Department of Chemistry, The University of North Carolina at Chapel Hill, Chapel Hill, North Carolina 27514. *Received November 14, 1986*

Abstract: Described are the synthesis of a tris(imidazole) chelating agent, timm, and the structure of its subsequently generated Cu(I) complex. The latter species is a dimer, $[Cu(timm)^+]_2$ (**1**), and its structure is compared with those of related copper(I) dimers. We also report the solution spectroscopic and photophysical properties of several copper(I) imidazole complexes including $Cu(timm)^+$ and its carbonyl adduct $Cu(timm)CO^+$. From these data, we propose a structure for the active site in HcCO which is consistent with (1) the structure deduced from protein crystallography and EXAFS spectroscopy, (2) the photophysical behavior of HcCO, and (3) the observed stoichiometry of CO binding by deoxyHc. Crystal data for **1**: monoclinic, $a = 8.515$ (4) Å, $b = 16.133$ (5) Å, $c = 13.054$ (5) Å, $\beta = 92.38$ (4)°, $V = 1792$ (2) Å^3, space group $P2_1/c$, and $Z = 4$.

Previous studies on the electronic absorption and photophysical properties of copper(I) pyrazole complexes[2] suggested to us that a similar investigation of copper(I) imidazole complexes might be useful for probing the coordination environment of copper proteins in which the metal ions were ligated by histidine. This notion, founded on the observation that the carbonyl derivative of hemocyanin (HcCO)[3] displays a luminescence at 550 nm,[4] was strengthened by a report in 1984 of the preliminary X-ray crystal structure of deoxyhemocyanin (deoxyHc) isolated from the arthropod *Panularis interruptus*.[5] The structure shows that only three imidazole residues are within bonding distance of each copper(I) ion.

In order to compare the photophysical properties of copper(I) imidazole complexes with those for the reduced forms of hemocyanin, we focused on compounds having no ligands besides imidazole. We have previously prepared several two-coordinate Cu(I) complexes,[6] but we lacked well-defined three-coordinate species.

(1) Fellow of the Alfred P. Sloan Foundation, 1985-1987.
(2) Sorrell, T. N.; Borovik, A. S. *Inorg. Chem.*, in press.
(3) Abbreviations used in this paper include the following: Hc, hemocyanin; HcO_2, oxyhemocyanin; HcCO, the carbonyl derivative of hemocyanin; deoxyHc, deoxyhemocyanin; pz, pyrazole; im, imidazole; 1,2-DMIm, 1,2-dimethylimidazole; timm, tris[2-(1-methylimidazolyl)]methoxymethane.
(4) Finazzi-Agro, A.; Zolla, L.; Flamigni, L.; Kuiper, H. A.; Brunori, M. *Biochemistry* **1982**, *21*, 415.
(5) (a) Gaykema, W. P. J.; Hol, W. G. J.; Verijken, J. M.; Soeter, N. M.; Bok, H. J.; Beintema, J. J. *Nature (London)* **1984**, *309*, 23. (b) Linzen, B.; Soeter, N. M.; Riggs, A. F.; Schneider, H.-J.; Schartau, W.; Moore, M. D.; Yokota, E.; Behrens, P. Q.; Nakashima, H.; Takagi, T.; Nemoto, T.; Verijken, J. M.; Bak, H. J.; Beintema, J. J.; Volbeda, A.; Gaykema, W. P. J.; Hol, G. W. J. *Science (Washington, D.C.)* **1985**, *229*, 519.
(6) Sorrell, T. N.; Jameson, D. J. *J. Am. Chem. Soc.* **1983**, *105*, 6013.

0002-7863/87/1509-4255$01.50/0